Functional analysis of transdifferentiated cardiomyocytes

Seven days after the cardiomyogenic induction, action potential (AP) was measured by use of standard glass microelectrodes, as described previously (17,18,20,21). Immediately after the recording, Alexa 568 was injected into the cell via recording microelectrodes to confirm that the recording AP was obtained from EGFP-positive human cells. Since thyroxin may affect the AP morphology, the medium was exchanged for a thyroxin-free medium 2 days before the AP recording. The extent of dye transfer was monitored under a fluorescent microscope, and digital images were recorded with a digital camera.

The fluorescent image of spontaneously beating EMC-derived cardiomyocytes was monitored using a CCD camera and was stored as digital video. The images of EMCs at day 7, 14, and 21 of co-culture in 10% FBS and FBS-free medium were recorded; then the cell contraction was analyzed using an image edge detection program made by Igor Pro 4 (Wavemetrics, Inc., Lake Oswego, OR, USA).

RNA extraction and reverse transcriptase (RT)-PCR

RT-PCR was done as described previously (17,18,20,21). Primers for the following genes were used: cardiac transcription factors—Csx/Nkx-2.5; cardiac structural proteins—cardiac troponin-I (cTnI) and cardiac troponin-T (cTnT). The internal control was 18s rRNA. PCR primers were prepared such that they would amplify the human but not the mouse genes.

Statistical analysis

Data were expressed as the mean ± SE. The difference between the two groups was determined with Student's *t*-test. Statistical significance was set at $P < 0.05$.

RESULTS

EGFP-labeled EMC100s, EMC214s, and MMCs cultured in either 10% FBS or FBS free started beating 3 days after the cardiomyogenic induction.

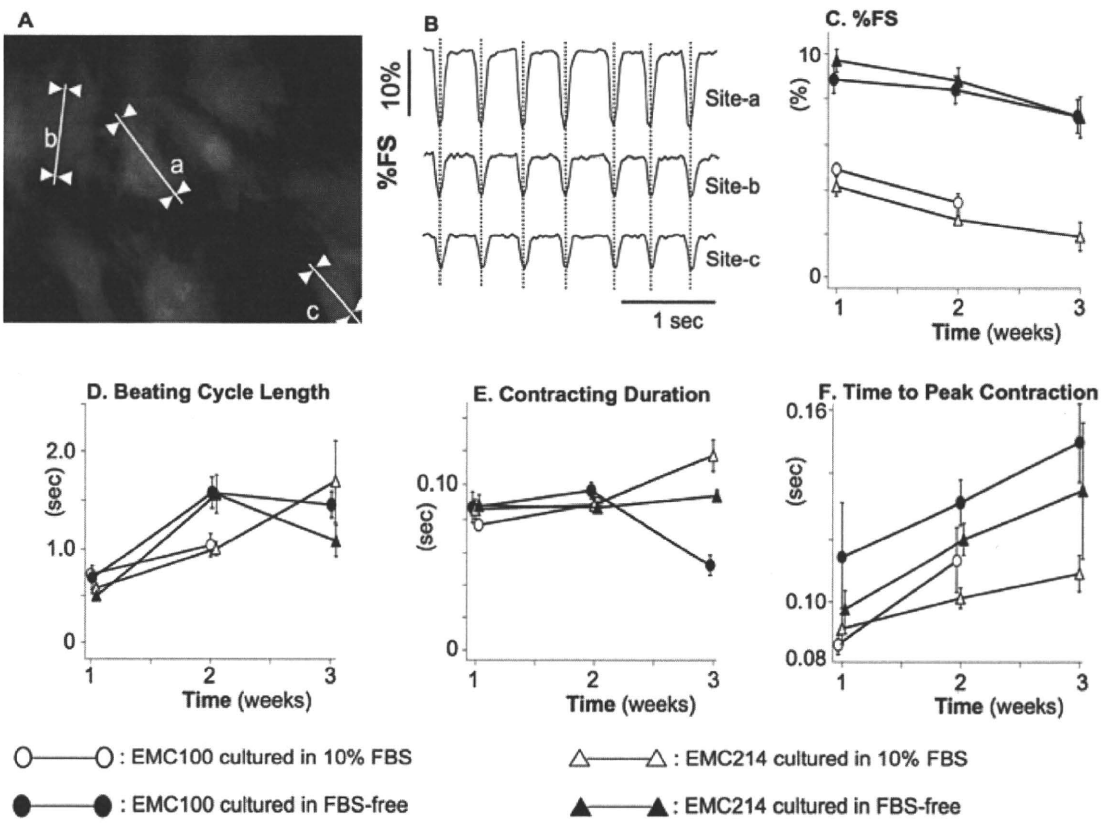

FIG. 1. Contraction parameter of EMC100 and EMC214-derived cardiomyocytes. (A) A representative fluorescent microscopic image of EMC-derived cardiomyocytes and detected fractional shortening (%FS) along the white line obtained from sites a, b, c are shown in (B). (C–F) Calculated contraction parameters are averaged as a function of time after cardiomyogenic induction. %FS cultured in FBS-free ACCITT are significantly greater than %FS cultured in DMEM with 10% FBS.

The EGFP-labeled human cells beat strongly in a synchronized manner on day 5 and continued to contract at least until day 21.

Functional analysis of differentiated EMCs

We analyzed the parameters of cell contraction using an image edge detection program. Edges were selected along the long axis of the EGFP-positive cells (Fig. 1A). The recorded contraction pattern showed synchronous beating of the cells (Fig. 1B). %FS of EMCs cultured in FBS-free medium was larger than that of EMCs cultured in 10% FBS medium. This difference was statistically significant and lasted until day 21 of co-culture. Other parameters—beating cycle length, contracting duration, and time to peak contraction—were not statistically significant, except contraction duration of EMC214s on day 21 of co-culture, which was observed to be significantly longer in FBS-free medium (Fig. 1C–F).

APs from 60 spontaneously beating EGFP-positive EMC214s were obtained. There was no difference in the observed AP morphological category, i.e., sinus node-like and working cardiomyocyte-like AP, between the 10% FBS and FBS-free medium (Fig. 2A–D). However, the maximum diastolic potential was significantly hyperpolarized, and the amplitude was greater in the FBS-free medium than in 10% FBS medium (Fig. 2E). AP duration more than 250 ms was only observed in FBS-free medium (0/41 vs. 3/19). The Alexa 568 dye spread into the GFP-positive adjacent EMCs, while not diffusing into the GFP-negative murine cardiomyocytes, suggesting there was no heterologous cell-to-cell gap connection, but that there was a homologus connection among EMCs in vitro (Fig. 2F–I).

FBS-free culture increased the cardiomyogenic transdifferentiation rate of EMCs and MMCs

The fraction of human cardiac troponin-I positive cells among the EGFP-positive cells was defined as the cardiomyogenic transdifferentiation rate (Fig. 3A–C). While EMCs and MMCs without co-culture did not show any troponin-I expression, EMCs and MMCs became positive for human cardiac troponin-I antibody as a result of the co-culture. The efficiency of cardiomyogenic transdifferentiation of EMC100s and MMCs was significantly increased (36 and 163%, respectively) as the result of cultivation

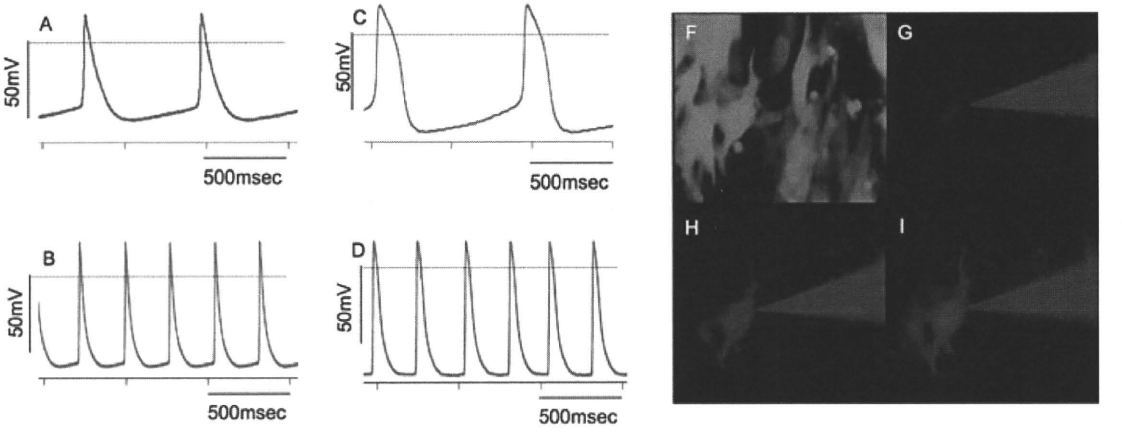

E

	Amplitude (mV)	MDP (mV)	APD90 (msec)	Vmax (V/sec)	n
10% FBS	66.5 ± 1.4	-53.1 ± 0.9	159.9 ± 4.9	9.46 ± 0.02	41
FBS-free	74.5 ± 2.6*	-57.3 ± 1.1*	179.6 ± 19.5	10.71 ± 1.31	19

DMP : Maximum Diastolic Potential
APD : Action Potential Duration
Mean ± SE

FIG. 2. Electrophysiological parameter of EMC214-derived cardiomyocytes. (A–D) A representative action potential (AP) shape of EMC214-derived cardiomyocytes. AP cultured by DMEM with 10% FBS showed triangular action potential shapes in AP with marked pacemaker-like potential (A) and without pacemaker-like potential (B). On the other hand, AP cultured with FBS-free ACCITT medium showed a prominent plateau in AP with pacemaker-like potential (C) and without it (D). (F) EGFP-labeled EMCs (green) were injected with Alexa 568 solution (red). (G–I) through a microelectrode to confirm that the recorded signal was obtained from EMCs. G, H, and I are sequential images as a function of time after dye transfer (0, 2, and 5 min after the dye transfer, respectively). Measured action potential parameters are averaged and shown in panel E.

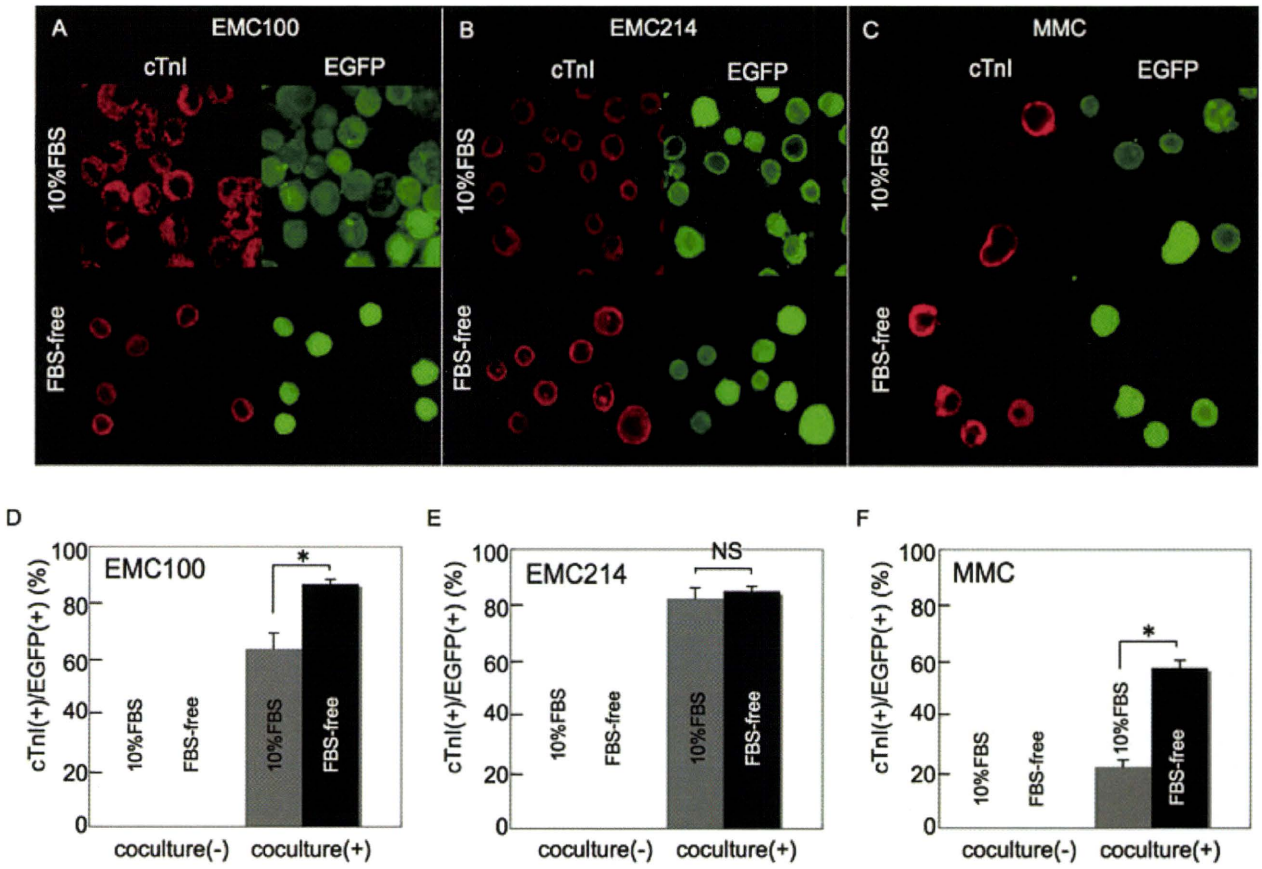

FIG. 3. Facilitating cardiomyogenic transdifferentiation efficiency of EMCs and MMCs by use of FBS-free ACCITT medium. (A–C) Representative immunocytochemical images are shown. Isolated EGFP-positive (green) EMC100s (A), EMC214s (B), and MMCs (C) with co-cultivation with murine cardiomyocytes by 10%FBS containing DMEM (DMEM) or FBS-free ACCITT medium (ACCITT) were stained with anticardiac troponin-I antibody (cTnI; red). (D–F) Cardiomyogenic transdifferentiation efficiency is defined as a proportion of cTnI-positive cells in EGFP-positive cells and averaged data are shown. ACCITT significantly increased the transdifferentiation efficiency of EMC100s and MMCs.

with FBS-free medium (Fig. 3D,F). Since the induction rate was saturated in the EMC214s (more than 80%), FBS-free medium tended to increase the cardiomyogenic induction rate of EMC214s; however, it is not statistically significant (Fig. 3E).

Immunocytochemistry

Immunocytochemical staining was done at day 7 of cardiomyogenic induction. EGFP-positive EMCs, when cultured in either medium, are positive for cardiac troponin-I (Fig. 4), α-actinin, and connexin 43 (Fig. 5). Cardiac troponin-I and α-actinin showed clear striation patterns, which indicated that differentiated EMCs were physiologically functioning. In the FBS-free medium, EMC-derived rod-shaped cardiomyocytes could be observed frequently (Fig. 4I–L). Connexin 43 was stained at the margin of α-actinin positive EMC-derived cardiomyocytes, suggesting tight electrical communication between the EMCs.

RT-PCR

EMCs constitutively expressed some cardiomyocyte-specific genes (18). In the present study, we confirmed that the FBS-free medium does not affect the mRNA expression of Nkx2.5, cardiac troponin I, cardiac troponin T, and cardiac actin at the default state (Fig. 6). These cardiomyocyte-specific genes were constitutively expressed before and after the cardiomyogenic induction.

DISCUSSION AND CONCLUSIONS

Serum-independent cardiomyogenic transdifferentiation of EMCs and MMCs

One of the most important findings in the present study is that serum in the culture medium is not an essential factor for cardiomyogenic transdifferentiation in human mesenchymal cells.

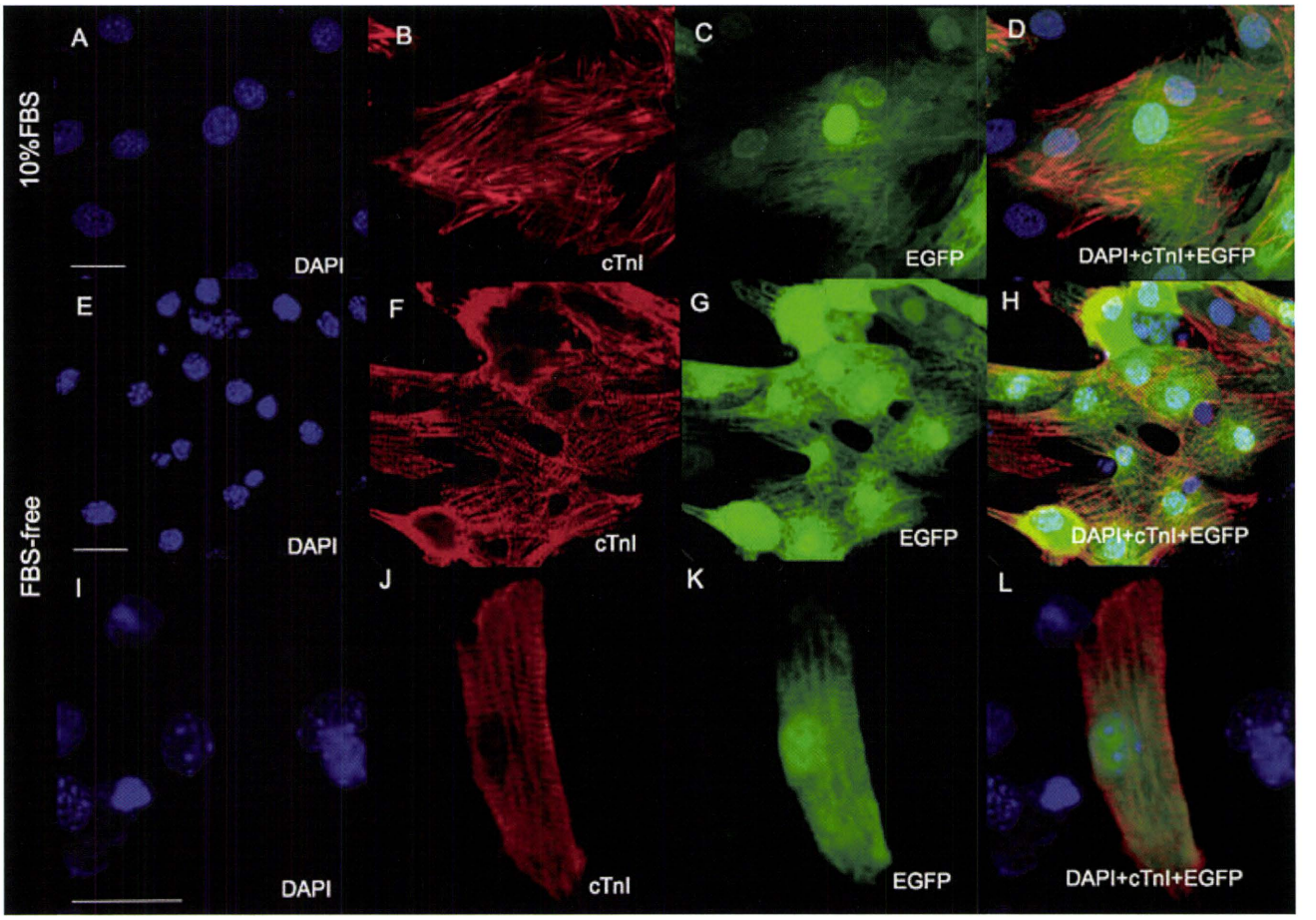

FIG. 4. Confocal microscopic view of EMC214-derived cardiomyocyte immunostained with anticardiac troponin-I antibody. Immunocytochemistry of transdifferentiated EMC214s with anticardiac troponin-I (cTnI) antibody. The cells were stained with DAPI (blue) and anti cTnI antibody (red). EGFP-positive (green) human EMC214s expressed cTnI. Note the clear striation staining pattern of EMC214s. Scale bar denotes 20 μm. Both EMC214s cultured with 10%FBS containing DMEM or FBS-free ACCITT medium expressed cTnI. EMC214s cultured with ACCITT medium sometimes showed a rod shape. Scale bar denotes 20 μm.

Several stem cell types are used for clinical patients. Of these stem cells, mesenchymal cells are reported to show cardiomyogenesis in vitro (16, 17), while others fail to show evidence of cardiomyogenesis in the experimental condition (22–24). There are preclinical candidates for stem cell sources that have cardiomyogenic ability (e.g., embryonic stem cells, cardiac presursor cells, etc.) (1,2,5,7,8,25); however, they may not be used for clinical patients, since clinical application has several problems. Thus, the analysis of key mechanisms for cardiomyogenic transdifferentiation in the human mesenchymal cell is important in order to expand the efficacy of current cardiac stem cell therapy. For cardiomyogenic transdifferentiation in the human mesenchymal cell, environmental factors, e.g., co-cultivation with cardiomyocytes obtained from other species (feeder cardiomyocytes), were reported as essential in the previous study (17). Feeder cardiomyocytes may secrete a humoral factor for cardiomyogenic transdifferentiation in human mesenchymal cells in vitro. Definition of these cardiomyogenic transdifferentiation factors in vitro are important, because it may improve the cardiomyogenic transdifferentiation efficiency of engrafted mesenchymal cells in vivo, and consequently, improve the efficacy of current cardiac stem cell therapy. The conventional culture medium, however, contains serum, which has numerous humoral factors that preclude the reliable detection of feeder-derived cardiomyogenic transdifferentiation factors. Thus, our serum-independent cardiomyogenic assay system may provide an effective model for identifying feeder-derived cardiomyogenic transdifferentiation factors in vitro. Furthermore, it is also important to state that serum in the culture medium does not play an essential role in cardiomyogenic transdifferentiation of human mesenchymal stem cells in vitro.

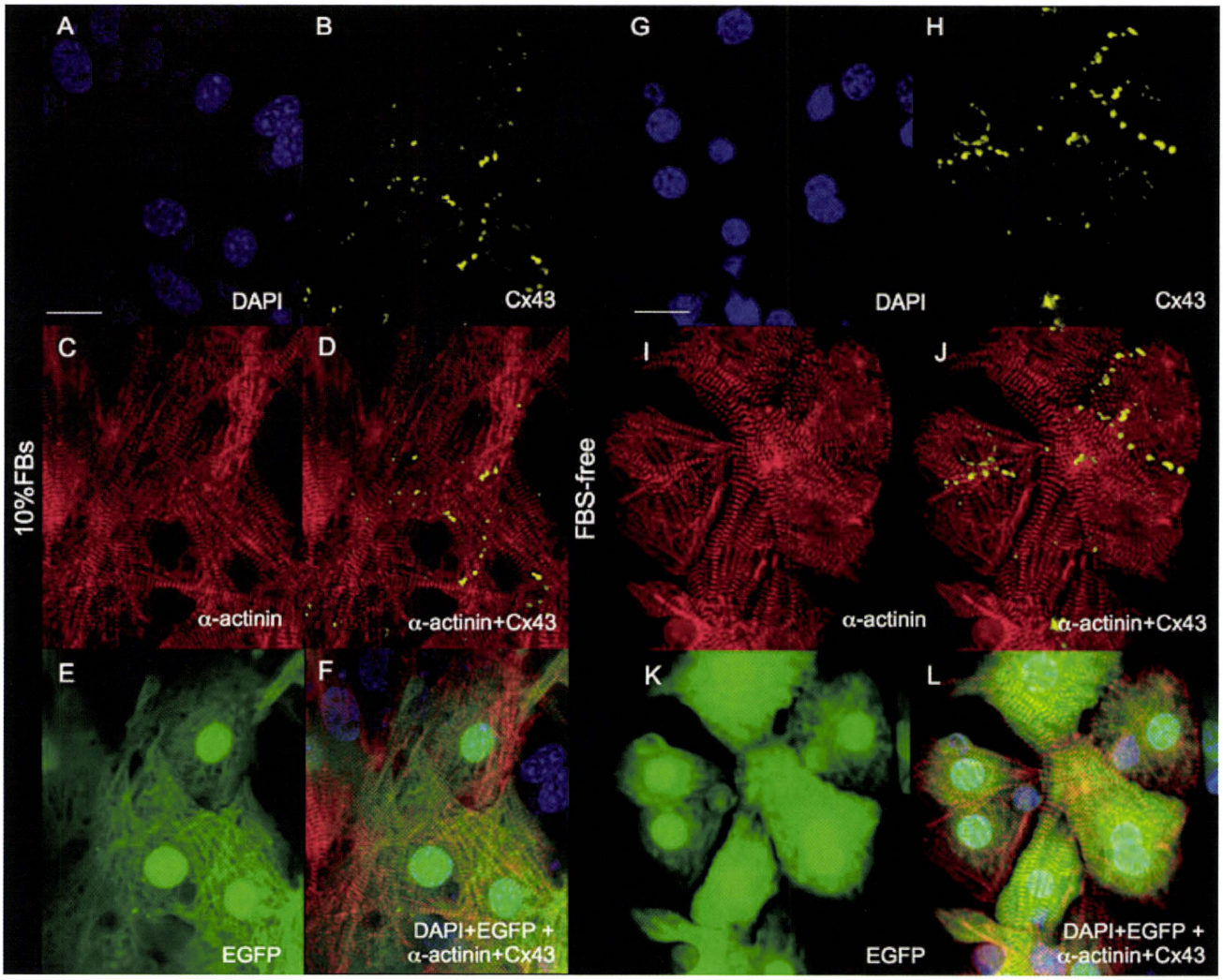

FIG. 5. Confocal microscopic view of EMC214-derived cardiomyocytes immunostained with anti-sarcomeric α-actinin and connexin 43 antibody. Immunocytochemistry of transdifferentiated EMC214s with anti-sarcomeric α-actinin (α-actinin) and connexin 43 (Cx43) antibody. The cells were stained with DAPI (blue), anti-α-actinin (red), and Cx43 (yellow) antibody. Both EMC214s cultured with 10%FBS containing DMEM or FBS-free ACCITT medium expressed α-actinin and Cx43. Scale bar denotes 20 μm.

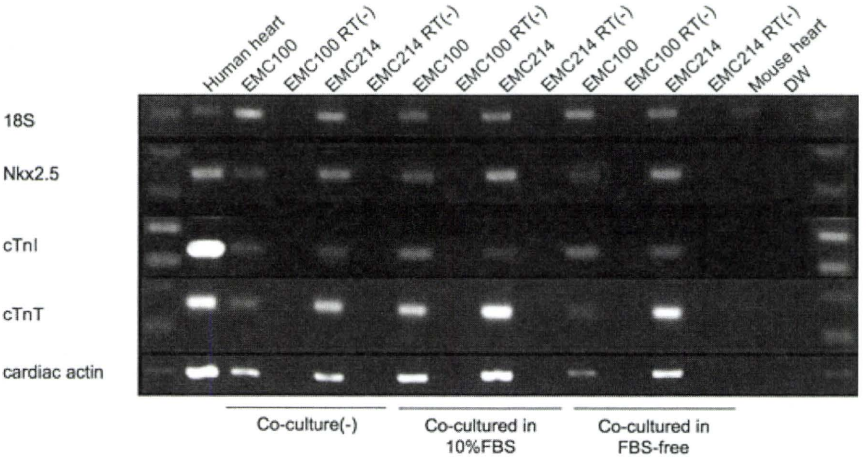

FIG. 6. Expression of cardiomyocyte-specific genes of EMC100 and MC214. RT-PCR was performed with PCR primers with specificity for human genes encoding cardiac proteins but not for the corresponding murine genes. Human heart and mouse heart cells were used as a positive control and negative control, respectively. Most human cardiac genes were constitutively expressed in the default state of EMCs and were not affected by FBS-free ACCITT medium.

Mechanism of improvement in cardiomyogenic transdifferentiation in FBS-free medium

FBS-free ACCITT medium was defined in the early 1990s (19,26) for culturing isolated adult rat ventricular myocytes. Since about 70% of the energy source for ATP production in the adult cardiomyocyte is free fatty acid, ACCITT medium contains L-carnitine, which is of central importance in mitochondrial fatty acid metabolism, in order to maintain an adult cardiomyocyte phenotype in situ. In the present study, both physiological and histological phenotypes in the differentiated cardiomyocytes from EMCs were more matured and maintained for a longer period in FBS-free medium than in 10% FBS-containing medium. Cardiomyogenic transdifferentiation efficiency of EMC100s and MMCs was significantly improved. The lack of statistical significance in the improvement of cardiomyogenic transdifferentiation efficiency of EMC214s may be due to extremely high cardiomyogenic transdifferentiation ability of EMC214s in 10%FBS medium. Consequently, the effect of FBS-free medium may be saturated in our system. In addition to adult myocytes in culture, FBS-free ACCITT may provide a suitable condition for maturation of EMC-derived and MMC-derived cardiomyocytes.

In order to define the essential element for facilitating cardiomyogenic transdifferentiation in FBS-free medium, we have tried to culture with FBS-free ACCITT medium, eliminating each element one by one; however, each element in ACCITT is essential for maintaining healthy feeder cardiomyocyte conditions, and the essential elements for facilitating cardiomyogenic transdifferentiation in ACCITT are still unclear. Alternatively, it is possible that 10% FBS inhibits cardiomyogenic transdifferentiation of EMCs and MMCs in the co-culture system. The mechanisms of improvement in cardiomyogenic transdifferentiation in FBS-free medium are still unclear. However, supplemental composition in ACCITT may be a clue to define factors that facilitate cardiomyogenic transdifferentiation in human mesenchymal cells. Further experiments should be done.

Establishment of a FBS-free cardiomyogenic transdifferentiation assay system in vitro

In our co-cultivation system, administration of the supernatant of murine cardiomyocyte culture did not cause cardiomyogenic transdifferentiation. Thus, the key factor for cardiomyogenic transdifferentiation may not be a humoral factor, but may be due to interaction between the mesenchymal cells and murine cells. Furthermore, the concentration of the factor secreted from the murine cardiomyocyte may not diffuse far; therefore, concentration of the specific factor could not be detected in the net supernatant of the culture medium. By use of a FBS-free cardiomyogenic transdifferentiation assay system, we may able to detect small concentration changes in the specific factors in the culture that may be masked when serum-containing medium is used in the assay system.

Acknowledgments: The research was partially supported by a grant from the Ministry of Education, Science and Culture, Japan. A part of this work was examined at the Keio Integrated Medical Research Center.

REFERENCES

1. Klug MG, Soonpaa MH, Koh GY, Field LJ. Genetically selected cardiomyocytes from differentiating embryonic stem cells form stable intracardiac grafts. *J Clin Invest* 1996;98:216–24.
2. Min JY, Yang Y, Converso KL, et al. Transplantation of embryonic stem cells improves cardiac function in post-infarcted rats. *J Appl Physiol* 2002;92:288–96.
3. Gojo S, Gojo N, Takeda Y, et al. In vivo cardiovasculogenesis by direct injection of isolated adult mesenchymal stem cells. *Exp Cell Res* 2003;288:51–9.
4. Shake JG, Gruber PJ, Baumgartner WA, et al. Mesenchymal stem cell implantation in a swine myocardial infarct model: engraftment and functional effects. *Ann Thorac Surg* 2002;73:1919–25; discussion 26.
5. Wang JS, Shum-Tim D, Galipeau J, Chedrawy E, Eliopoulos N, Chiu RC. Marrow stromal cells for cellular cardiomyoplasty: feasibility and potential clinical advantages. *J Thorac Cardiovasc Surg* 2000;120:999–1005.
6. Koyanagi M, Urbich C, Chavakis E, et al. Differentiation of circulating endothelial progenitor cells to a cardiomyogenic phenotype depends on E-cadherin. *FEBS Lett* 2005;579: 6060–6.
7. Beltrami AP, Barlucchi L, Torella D, et al. Adult cardiac stem cells are multipotent and support myocardial regeneration. *Cell* 2003;114:763–76.
8. Oh H, Bradfute SB, Gallardo TD, et al. Cardiac progenitor cells from adult myocardium: homing, differentiation, and fusion after infarction. *Proc Natl Acad Sci USA* 2003;100: 12313–8.
9. Chen SL, Fang WW, Ye F, et al. Effect on left ventricular function of intracoronary transplantation of autologous bone marrow mesenchymal stem cell in patients with acute myocardial infarction. *Am J Cardiol* 2004;94:92–5.
10. Assmus B, Schachinger V, Teupe C, et al. Transplantation of progenitor cells and regeneration enhancement in acute myocardial infarction (TOPCARE-AMI). *Circulation* 2002;106: 3009–17.
11. Hamano K, Nishida M, Hirata K, et al. Local implantation of autologous bone marrow cells for therapeutic angiogenesis in patients with ischemic heart disease: clinical trial and preliminary results. *Jpn Circ J* 2001;65:845–7.
12. Strauer BE, Brehm M, Zeus T, et al. Repair of infarcted myocardium by autologous intracoronary mononuclear bone marrow cell transplantation in humans. *Circulation* 2002;106: 1913–8.
13. Menasche P, Hagege AA, Scorsin M, et al. Myoblast transplantation for heart failure. *Lancet* 2001;357:279–80.

14. Tang YL, Zhao Q, Zhang YC, et al. Autologous mesenchymal stem cell transplantation induce VEGF and neovascularization in ischemic myocardium. *Regul Pept* 2004;117:3–10.
15. Gnecchi M, He H, Liang OD, et al. Paracrine action accounts for marked protection of ischemic heart by Akt-modified mesenchymal stem cells. *Nat Med* 2005;11:367–8.
16. Makino S, Fukuda K, Miyoshi S, et al. Cardiomyocytes can be generated from marrow stromal cells in vitro. *J Clin Invest* 1999;103:697–705.
17. Takeda Y, Mori T, Imabayashi H, et al. Can the life span of human marrow stromal cells be prolonged by bmi-1, E6, E7, and/or telomerase without affecting cardiomyogenic differentiation? *J Gene Med* 2004;6:833–45.
18. Hida N, Nishiyama N, Miyoshi S, et al. Novel cardiac precursor-like cells from human menstrual blood-derived mesenchymal cells. *Stem Cells* 2008;26:1695–704.
19. Ellingsen O, Davidoff AJ, Prasad SK, et al. Adult rat ventricular myocytes cultured in defined medium: phenotype and electromechanical function. *Am J Physiol* 1993;265:H747–54.
20. Nishiyama N, Miyoshi S, Hida N, et al. The significant cardiomyogenic potential of human umbilical cord blood-derived mesenchymal stem cells in vitro. *Stem Cells* 2007;25:2017–24.
21. Okamoto K, Miyoshi S, Toyoda M, et al., 'Working' cardiomyocytes exhibiting plateau action potentials from human placenta-derived extraembryonic mesodermal cells. *Exp Cell Res* 2007;313:2550–62.
22. Balsam L, Wagers A, Christensen J, Kofidis T, Weissman I, Robbins R. Haematopoietic stem cells adopt mature haematopoietic fates in ischaemic myocardium. *Nature* 2004;428:668–73.
23. Murry C, Soonpaa M, Reinecke H, et al. Haematopoietic stem cells do not transdifferentiate into cardiac myocytes in myocardial infarcts. *Nature* 2004;428:664–8.
24. Murry CE, Wiseman RW, Schwartz SM, Hauschka SD. Skeletal myoblast transplantation for repair of myocardial necrosis. *J Clin Invest* 1996;98:2512–23.
25. Orlic D, Kajstura J, Chimenti S, et al. Bone marrow cells regenerate infarcted myocardium. *Nature* 2001;410:701–5.
26. Volz A, Piper HM, Siegmund B, Schwartz P. Longevity of adult ventricular rat heart muscle cells in serum-free primary culture. *J Mol Cell Cardiol* 1991;23:161–73.

Gen Thorac Cardiovasc Surg (2010) 58:194–196
DOI 10.1007/s11748-009-0507-0

CASE REPORT

Repair of traumatic tricuspid insufficiency via minimally invasive port access

Hirofumi Kasahara, MD · Mikihiko Kudo, MD
Hiroyuki Kawajiri, MD · Ryohei Yozu, MD

Received: 27 May 2009 / Accepted: 3 July 2009

Abstract We report on a successful tricuspid valve plasty using port-access minimally invasive cardiac surgery (MICS) for severe traumatic tricuspid insufficiency caused by blunt chest trauma suffered 15 years previously. A combination repair procedure, consisting of cleft closures, plication of the anteroseptal commissure, and ring annuloplasty, was necessary to achieve valve competence and proved possible via port access without difficulty. Port-access MICS is an alternative approach for tricuspid valve surgery.

Key words Traumatic tricuspid insufficiency · Port access · Minimally invasive cardiac surgery

Introduction

Minimally invasive mini-thoracotomy is now used regularly in cardiac surgery to avoid potential median sternotomy-related complications. Surgical trauma to the patient can be reduced without compromising quality or safety and leads to faster recovery.[1,2] In addition, a small submammary incision results in improved cosmesis, especially for female patients. We herein describe a patient with severe traumatic tricuspid insufficiency (TI) that was corrected via this approach.

H. Kasahara (✉) · M. Kudo · H. Kawajiri · R. Yozu
Department of Surgery, School of Medicine, Keio University, 35 Shinano-machi, Shinjuku-ku, Tokyo 160-8582, Japan
Tel. +81-3-3353-1216; Fax +81-3-5379-3034
e-mail: kasahara@sc.itc.keio.ac.jp

Case report

A 46 year-old woman whose case had been followed for several years at another hospital with a diagnosis of severe traumatic TI was referred to our hospital for a cardiac operation because she had become more breathless during exercise. She had a history of blunt chest trauma due to a traffic accident 15 years previously that had resulted in 24 rib fractures. On admission to our hospital, electrocardiography showed an incomplete right bundle branch block with normal sinus rhythm. Echocardiography revealed severe TI, chiefly resulting from failed valves and chordae ruptures of the anterior tricuspid leaflet, plus right ventricular dilatation.

Operative technique

Cardiac exposure was obtained through a right anterior mini-thoracotomy with a 7-cm submammary incision by means of port-access minimally invasive cardiac surgery (MICS), as has been previously reported.[3,4] Briefly, the femoral artery and vein were used to establish cardiopulmonary bypass (CPB) using Fem-Flex II cannulas (Edwards Lifesciences, Midvale, UT, USA) via a small groin incision. A soft vent catheter was inserted via the right upper pulmonary vein. Aortic cross-clamping was applied using a modified Cosgrove flex clamp via the port, and cardiac arrest was achieved by antegrade cardioplegia using a root cannula and topical cooling. The tricuspid valve (TV) and subvalvular apparatus were observed after a tracheal tube was inserted into the superior vena cava via right atriotomy to establish total CPB. Several chordae ruptures, with a large cleft on the anterior leaflet of the TV, were observed. Cleft closure

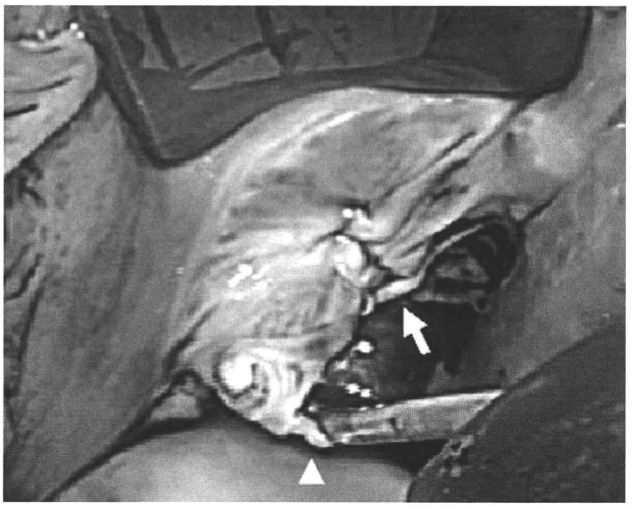

Fig. 1 Intraoperative findings show massive tricuspid regurgitation, chiefly due to failed valves and chordae ruptures of the anterior leaflet on the tricuspid valve. A large cleft on the anterior leaflet was closed by means of a continuous suture (*arrow*). A severely failed valve with chordae rupture (*arrowhead*) remains, however, especially around the anteroseptal commissure (indicated by a hook)

from the free edge with a continuous suture was performed (Fig. 1). Plication of the partial anteroseptal commissure was performed due to extremely poor coaptation, taking care to avoid creating TV stenosis. Ring annuloplasty was also carried out using a 28-mm Edwards MC3 annuloplasty system (Edwards Lifesciences, Irvine, CA, USA). A water test showed a dramatic reduction of TI. However, a mild degree of TI remained due to a small cleft in the center of the septal leaflet of the TV. TI disappeared after cleft closure using the same technique. The postoperative course was uneventful, and the patient was discharged 7 days after the operation. Postoperative echocardiography revealed trivial TI.

Discussion

There are few reports regarding TV surgery using port-access MICS, but this technique enables good exposure. Advantages of the port-access approach include reduction of surgical trauma, due in part to less blood loss, and earlier recovery to full activity, as well as avoidance of median sternotomy-related complications, such as deep wound infection, compromised cosmesis, and possible injury to the right ventricle during repeated sternotomy.[1–3] Limitations of this approach include concomitant cardiac or aortic procedures other than mitral disease or simple congenital defects. A patient with a high likelihood of dense lung adhesions is also contraindicated for this approach due to technical difficulties. Based on our experience of more than 400 cases using this approach, we currently prefer using a flexible metal clamp instead of balloon aortic occlusion to secure clamping and to avoid balloon migration. Transesophageal echocardiography is also essential to evaluate whether there is aortic insufficiency or left ventricular distention during the infusion of cardioplegic solution, as when using mini-thoracotomy the left side of the heart cannot be seen. In the present case, there were minor concerns about lung adhesions due to the multiple rib fractures, but they proved trivial and the procedure was performed without difficulty.

Traumatic TI is a relatively rare complication of blunt chest trauma; but due to the increasing sophistication of imaging facilities, reports on the discovery of this particular disease have become more common in the literature. Traumatic TI due to complex lesions, often consisting of ruptured chordae, torn leaflets, and cusp retraction, is still a challenging surgical problem, being different from TI caused by simple annular dilatation secondary to mitral disease.[5] Several techniques have been reported—including artificial chordae implants, papillary muscle reconstruction, double orifices, clover technique, and bicuspidization—that avoid prosthesis-related complications and long anticoagulation treatment and that preserve the geometry and function of the right ventricle.[5,6] Repair is preferable to replacement with prostheses. We believe that the above techniques can be applied via port access in addition to the conventional approach.

Conclusion

We have presented a successful TV repair using port-access MICS for severe traumatic TI caused by blunt chest trauma. Combination repair procedures were feasible via a less invasive port-access approach, making this technique a successful alternative to traumatic TV surgery and other TV procedures.

References

1. Kypson AP, Glower DD. Minimally invasive tricuspid operation using port access. Ann Thorac Surg 2002;74:43–5.
2. Dogan S, Aybek T, Risteski PS, Detho F, Rapp A, Wimmer-Greinecker G, et al. Minimally invasive port access versus conventional mitral valve surgery: prospective randomized study. Ann Thorac Surg 2005;79:492–8.
3. Yozu R, Shin H, Maehara T, Iino Y, Mitsumaru A, Kawada S. Port-access cardiac surgery: experience with 34 cases at Keio University Hospital. Jpn J Thorac Cardiovasc Surg 2001;49:360–4.

4. Yozu R, Shin H, Maehara T. Minimally invasive cardiac surgery by the port-access method. Artif Organs 2002;26: 430–7.
5. De Bonis M, Lapenna E, La Canna G, Grimaldi A, Maisano F, Torracca L, et al. A novel technique for correction of severe tricuspid valve regurgitation due to complex lesions. Eur J Cardiothorac Surg 2004;25:760–5.
6. Doi A, Takahara Y, Mogi K, Hatakeyama M. Repair of traumatic tricuspid regurgitation by bicuspidization. Gen Thorac Cardiovasc Surg 2007;55:499–501.

Photochemistry and Photobiology, 2011, 87: 199–207

Photosensitization Reaction-Induced Acute Electrophysiological Cell Response of Rat Myocardial Cells in Short Loading Periods of Talaporfin Sodium or Porfimer Sodium

Arisa Ito*[1], Takehiro Kimura[2], Shunichiro Miyoshi[2], Satoshi Ogawa[3] and Tsunenori Arai[1]

[1]School of Fundamental Science and Technology, Graduate School of Science and Technology, Keio University, Kohoku-ku, Yokohama, Japan
[2]Cardiopulmonary Division, Department of Internal Medicine, Keio University School of Medicine, Shinjuku-ku, Tokyo, Japan
[3]Mita Hospital, International University of Health and Welfare, Minato-ku, Tokyo, Japan

Received 8 August 2010, accepted 20 October 2010, DOI: 10.1111/j.1751-1097.2010.00846.x

ABSTRACT

Electrophysiological responses of rat myocardial cells to exogenous photosensitization reactions for a short period of incubation with two photosensitizers, talaporfin sodium or porfimer sodium, were measured in a subsecond time scale. The loading period of the photosensitizer when the photosensitizer might not be taken up by the cells was selected as 15 min, which was determined by the fluorescence microscopic observation. We measured the intracellular Ca^{2+} concentration ($[Ca^{2+}]_{in}$) by using a fluorescent Ca^{2+} indicator, Fluo-4 AM, under a high-speed confocal laser microscope to evaluate the acute electrophysiological cell response to the photosensitization reaction. The measured temporal change in Fluo-4 fluorescence intensity indicated that the response to the photosensitization reaction might be divided into two phases in both photosensitizers. The first phase is acute response: disappearance of Ca^{2+} oscillation when irradiation starts, which might be caused by ion channel dysfunction. The second phase is slow response: $[Ca^{2+}]_{in}$ elevation indicating influx of Ca^{2+} due to the concentration gradient. The continuous Ca^{2+} influx followed by changes in cell morphology suggested micropore formation on the surface of the cell membrane, resulting in necrotic cell death.

INTRODUCTION

Photosensitization reaction-induced cellular damage has been widely applied to clinical therapies such as noninvasive cancer therapy and age-related macular degeneration (1,2). Photochemical interactions involve photons, photosensitizers and oxygen generate reactive oxygen species, mainly singlet molecular oxygen (3–5). The activated singlet oxygen reacts with many biological molecules, including lipids, proteins and nucleic acids, resulting in apoptotic or necrotic cellular damage (6–8). The cellular response to photosensitization reaction is dependent on photosensitizer distribution, which is determined by the loading process and the physicochemical properties of the photosensitizer molecule, particularly molecular size, structure, charge and water solubility (9,10). The photosensitization reaction may cause selective organelle damage when the photosensitizer localizes to certain cellular compartments such as the mitochondria or lysosomes after a long incubation period (4,6). These damages to organelles may initiate enzyme activation followed by apoptosis. After a short incubation period of several minutes, the photosensitizer may not be taken up into the cells and may be distributed on the cell membrane or outside the cells (5). The membrane-bound photosensitizers irradiated by excitation light may induce membrane disruption, for example, due to micropore formation and ion channel dysfunction, resulting in morphological and electrophysiological changes in the cells (6,11).

Oxidative injury is known to be induced by exposure of cells to exogenous photosensitization reactions that increase intracellular free Ca^{2+} concentrations ($[Ca^{2+}]_{in}$) (12–14). The importance of Ca^{2+} for the viability and electrophysiological function of cells is well recognized (15,16). Ca^{2+} overload may play a role in photosensitization reaction-induced necrotic cell death (6). The intracellular Ca^{2+} dynamics during photosensitization reaction has been studied in various cell types such as erythrocytes (17), cardiomyocytes (18,19) and cancer cells (13,20). However, to our knowledge, there are no reports on the acute effect of exogenous photosensitization reactions on $[Ca^{2+}]_{in}$ in myocardial cells as observed in the subsecond scale.

In this study, we focused on the early events of Ca^{2+} dynamics during the onset of exogenous photosensitization reaction in short period of photosensitizer incubation. The photosensitization reaction was induced by short-time incubation of rat myocardial cells with two distinctive clinically approved photosensitizers, porfimer sodium and talaporfin sodium. Porfimer sodium (Photofrin®), a preparation of hematoporphyrin derivatives (HPD), is the most popular photosensitizer and has been applied to various therapies for malignant tumors (1,21). The lipophilic character of porfimer sodium may cause it to localize in the cell membrane and in the subcellular membrane. The cellular uptake of this photosensitizer has been studied in various types of tumor cells. Its subcellular pharmacokinetics in tumor cells is as follows:

*Corresponding author email: arisa.i@arai.appi.keio.ac.jp (Arisa Ito)

distribution on the cell membrane in the first several tens of minutes of incubation, slow uptake into the cells and then localization to other organelle membranes, especially the mitochondria, lysosome and Golgi apparatus in the final stage (22). The other photosensitizer used was the hydrophilic chlorin photosensitizer talaporfin sodium, also called mono-L-aspartyl chlorin e6 (NPe6), a chlorophyll derivative (1,23). Talaporfin sodium has been approved for early-stage lung cancer therapy in Japan as Laserphyrin® (24,25). Talaporfin sodium has been reported to localize to lysosomes after a long period of incubation (26–28). The change in intracellular Ca^{2+} concentration was measured using a high-speed confocal microscope with a frame rate of five frames per second to assess the electrophysiological cellular responses to photosensitization reactions with talaporfin sodium and porfimer sodium.

MATERIALS AND METHODS

Cell culture. Rat myocardial cells (Primary Cell Co., Ltd., Hokkaido, Japan) were cultured in Medium I (Dulbecco's modified Eagle's medium/nutrient mixture F-12 [D-MEM/F-12] supplemented with 10% fetal bovine serum, 100 U mL^{-1} penicillin and 100 $\mu g\ mL^{-1}$ streptomycin; all from Invitrogen, Carlsbad, CA) in an atmosphere of 95% air and 5% CO_2 at 37°C.

Photosensitizers. The photosensitization reaction was performed using two kinds of photosensitizers, a hydrophilic photosensitizer (talaporfin sodium) and a lipophilic photosensitizer (porfimer sodium). Talaporfin sodium (Meiji Seika Kaisha Ltd., Tokyo, Japan), 799.69 MW, has a major absorption peak of the Q band at 664 nm and an average molar absorbance of $2.7 \times 10^4\ M^{-1}\ cm^{-1}$ at 667 nm in a medium (without phenol red) containing 10% fetal bovine serum (29). Porfimer sodium (Wyeth Lederle, Japan Ltd., Tokyo, Japan), 1,231.28–4,883.30 MW, has a major absorption peak of Q band at 625 nm and an average molar absorbance of $2.9 \times 10^3\ M^{-1}\ cm^{-1}$ at 630 nm in the same mixture as mentioned above (29).

Photocytotoxic effect. The isolated rat myocardial cells were placed in collagen-coated 96 well microplates at a concentration of 2×10^4 cells per well and cultured in Medium I at 37°C in 5% CO_2. After 6–7 days in culture, the cells were loaded with 10–50 $\mu g\ mL^{-1}$ talaporfin sodium or porfimer sodium medium solution and kept in the dark for 30 min. After incubation in the dark, the cells were exposed to a 670 nm red diode laser (OpticalFuel; Sony Co., Ltd., Tokyo, Japan) for talaporfin sodium or 633 nm red diode laser (HPD 5215; Intense Ltd., NJ) for porfimer sodium at a fluence rate of 150 mW cm^{-2} and a total fluence of 1–10 J cm^{-2}. The cell lethality rate with the photosensitization reaction was measured using a water-soluble tetrazolium-8 (WST-8) assay kit (Cell Counting Kit-8; Doujinkagaku Co., Ltd., Kumamoto, Japan). After irradiation, the culture medium was replaced with a medium without the photosensitizer and 10 μL of WST-8 was added to the wells. After 2 h incubation, the absorbance of the reaction products at 450 nm was measured using a microplate absorbance reader (Sunrise™; Tecan Group Ltd., Maennedorf, Switzerland). The cell lethality rate was calculated as a percentage relative to the absorbance of living cells in the reference well without the photosensitization reaction. The absorbance of the complete viable cells (cell lethality rate of 0%) was defined as the difference between the absorbance of the cells with no irradiation without photosensitizer loading and that of the cells irradiated by 10 J cm^{-2} laser light after incubation with 50 $\mu g\ mL^{-1}$ talaporfin sodium or porfimer sodium. The normalized ratios characterized by the above definitions were used to calculate the cell lethality rate.

Subcellular distribution. The isolated rat myocardial cells were grown on 15 mm glass coverslips placed in a 35 mm petri dish 3 days before the experiment. The culture medium was replaced with 30 $\mu g\ mL^{-1}$ talaporfin sodium or porfimer sodium dissolved in Medium II (minimal essential medium supplemented with 10% fetal bovine serum; all from Invitrogen) and then the cells were further incubated for 15 min for 3 h in the dark. To determine the subcellular uptake of the two photosensitizers in rat myocardial cells, the cells incubated with the photosensitizers were stained with a lysosome probe (for talaporfin sodium) or mitochondria probe (for porfimer sodium), since it has been reported that talaporfin sodium localizes to the lysosome and porfimer sodium localizes to the mitochondrion after a long incubation period with tumor cells (10,22,30). After photosensitizer incubation, the cells were washed with the fresh medium without photosensitizer and loaded with a lysosome probe, 1 μM LysoTracker Green (Molecular Probes Inc., Eugene, OR), or mitochondria probe, 1 $\mu g\ mL^{-1}$ Rhodamine 123 (Molecular Probes Inc.) for an additional 30 min at room temperature. After staining, the medium was replaced with a fresh medium and the cells were placed on the stage of an inverted fluorescence microscope (BX51WI; Olympus Co., Ltd., Tokyo, Japan) equipped with ×40 water immersion lens (LUMPlanFL40 × W; Olympus Co., Ltd). Talaporfin sodium or porfimer sodium was excited at 400 ± 10 nm in the Solet band of these photosensitizers, using a 100 W mercury lamp with a band-pass filter, and the fluorescence was detected with a 600 nm long-pass filter. LysoTracker Green or Rhodamine 123 was excited by green light with a 470–495 nm band-pass filter, whereas a 510–550 nm band-pass filter was used to detect fluorescence. No interference was observed between the photosensitizers and organelle probe in the wavelengths used. Fluorescence images for both photosensitizers were taken using a near-infrared cooled CCD camera (Rolera-XR; QImaging, Burnaby, Canada). Image analysis was performed using ImageJ 1.41 (National Institute of Health, Bethesda, MD).

Intracellular Ca^{2+} concentration during the photosensitization reaction. Myocardial cells were grown on 15 mm glass coverslips placed in a 35 mm Petri dish for 2 days and then the change in intracellular free Ca^{2+} concentration ($[Ca^{2+}]_{in}$) during the exogenous photosensitization reaction was examined using a fluorescent Ca^{2+} indicator, Fluo-4 AM (Molecular Probes Inc). Fluo-4, a type of Fluo-4 AM hydrolyzed by cellular esterases inside the cells, has an absorption peak at 494 nm and a fluorescence peak at 516 nm (31,32); thus, the measurement of Fluo-4 fluorescence will not affect the photosensitization reaction. To measure the cellular response to the exogenous photosensitization reaction, in $[Ca^{2+}]_{in}$, the cells were loaded with 5 μM Fluo-4 AM dissolved in Medium II to a 2.2 mM total Ca^{2+} concentration in the medium for 20 min at room temperature. The medium was then replaced with 30 $\mu g\ mL^{-1}$ talaporfin sodium or porfimer sodium for an additional 15 min. In this loading condition of "short period of incubation," both talaporfin sodium and porfimer sodium may not be taken up into the cells. The reaction was observed under a fluorescence microscope to determine the subcellular photosensitizer localization. The amount of photosensitizer taken up into the cellular compartment in the 15 min loading period might be less than 1/10 of that in 30 min incubation for talaporfin sodium. Porfimer sodium has been reported to distribute on the cell membrane in less than 2 h of incubation (22). The cell response in the condition of "long period of photosensitizer incubation" was also measured to compare the cellular response between the loading periods of photosensitizer. A long loading period was determined to be 1 h for talaporfin sodium and 3 h for porfimer sodium. Figure 1 shows the experimental setup for the measurement of $[Ca^{2+}]_{in}$ in rat myocardial cells during the photosensitization reaction with talaporfin sodium or porfimer sodium. Fluo-4 in the myocardial cells was excited with an argon laser at 488 nm (800BL; National Laser Co., Salt Lake City, UT) and talaporfin sodium or porfimer sodium was excited at 655 ± 25 nm (103 mW cm^{-2}) or 625 ± 25 nm (117 mW cm^{-2}), respectively, using a 100 W mercury lamp with a band-pass filter. Fluo-4 fluorescence images were obtained with a confocal laser microscope system (CSU-X1; Yokogawa Electric Company, Tokyo, Japan) mounted on a differential interference microscope (BX51WI-FL-IRDIC; Olympus Co., Ltd) with ×40 water immersion lens. Fluo-4 fluorescence was detected at the 500–540 nm band-pass filter with an electron multiplication CCD camera (DU897; Andor Technology, Belfast, UK) with a frame rate of 200 ms per frame. The detected images were analyzed by the image software iQ Core (Andor Technology). The average Fluo-4 fluorescence intensity inside the cells was used to assess the changes in $[Ca^{2+}]_{in}$ in myocardial cells.

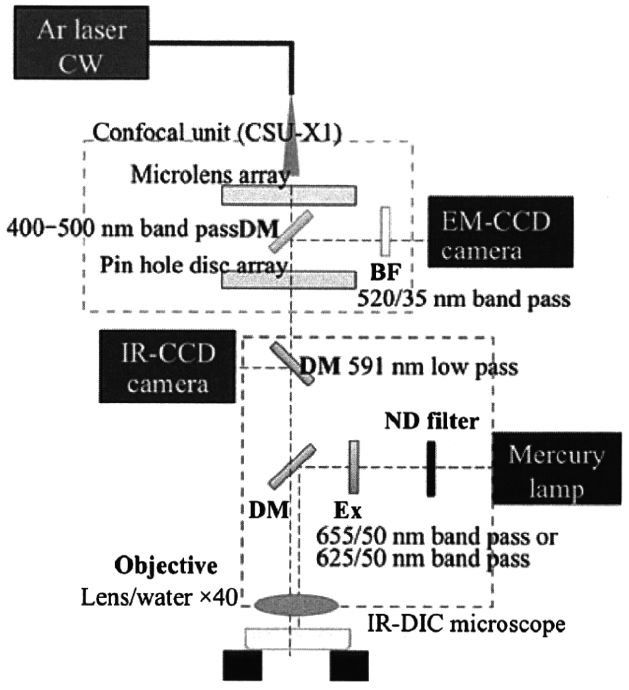

Figure 1. Experimental setup for the measurement of intracellular Ca^{2+} concentration in rat myocardial cells, using a high-speed confocal laser microscope during the photosensitization reaction with talaporfin sodium or porfimer sodium.

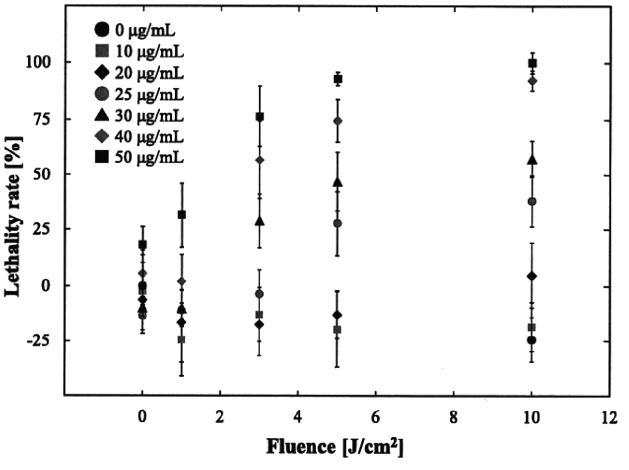

Figure 2. Cell lethality rate in the photosensitization reaction with talaporfin sodium was dependent on the fluence and photosensitizer concentration at the loading time of 30 min.

RESULTS

Photocytotoxic effect of photosensitization reaction with talaporfin sodium or porfimer sodium in rat myocardial cells

The examined parameters in the photosensitization reaction were photosensitizer concentration, laser light energy (in fluence, J cm^{-2}) and loading period. The variation in loading period induced little difference in photocytotoxicity. Figures 2 and 3 show the cell lethality change with fluence in various photosensitizer concentrations at the loading time of 30 min.

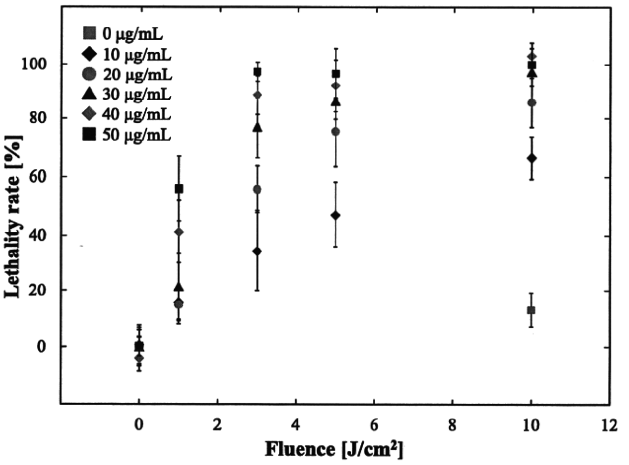

Figure 3. Cell lethality rate in the photosensitization reaction with porfimer sodium was dependent on the fluence and photosensitizer concentration at the loading time of 30 min.

The same tendency was observed in both photosensitizers; that is, the lethality rate increased with the increase in photosensitizer concentration and fluence. When the lethality rate was more than 50%, drastic morphological changes in cells were observed from the phase-contrast microscopic observation: first, a granulated cytoplasm, then bleb formation and finally cell shrinkage were seen. The photosensitizer concentration was selected as 30 $\mu g\ mL^{-1}$ for the subsequent study based on the following requirements: more than 50% lethality rate at 10 J cm^{-2} and monotonous increase in lethality up to 10 J cm^{-2}.

Subcellular distribution of talaporfin sodium or porfimer sodium in rat myocardial cells

The subcellular distribution of talaporfin sodium and porfimer sodium in rat myocardial cells with the short loading period of up to 1 h in talaporfin sodium and 3 h in porfimer sodium was determined using a fluorescence microscope. The bright-field image, talaporfin sodium fluorescence image, LysoTracker Green fluorescence image and the merged image of talaporfin sodium fluorescence (red) and LysoTracker Green fluorescence (green) using the same myocardial cells at the incubation times of 15 min, 30 min and 45 min are shown in Fig. 4a–l. In the fluorescence image of Fig. 4b, the narrow distribution of talaporfin sodium, unlike the LysoTracker fluorescence distribution (Fig. 4d), indicates that talaporfin sodium might not be taken up into the cells in the 15 min loading period. When cells were incubated with talaporfin sodium for 30–45 min, the photosensitizer fluorescence distribution corresponded with the LysoTracker Green fluorescence distribution (Fig. 4h,l), which indicates that talaporfin sodium was taken up into the myocardial cells and localized to the lysosome over the 30 min incubation time.

The bright-field image, porfimer sodium fluorescence image, Rhodamine 123 fluorescence image and the merged image of porfimer sodium fluorescence (red) and Rhodamine 123 fluorescence (green) using the same myocardial cells in incubation times of 30 min, 2 h and 3 h are shown in Fig. 5a–l. In the case of 30 min incubation (Fig. 5b), the

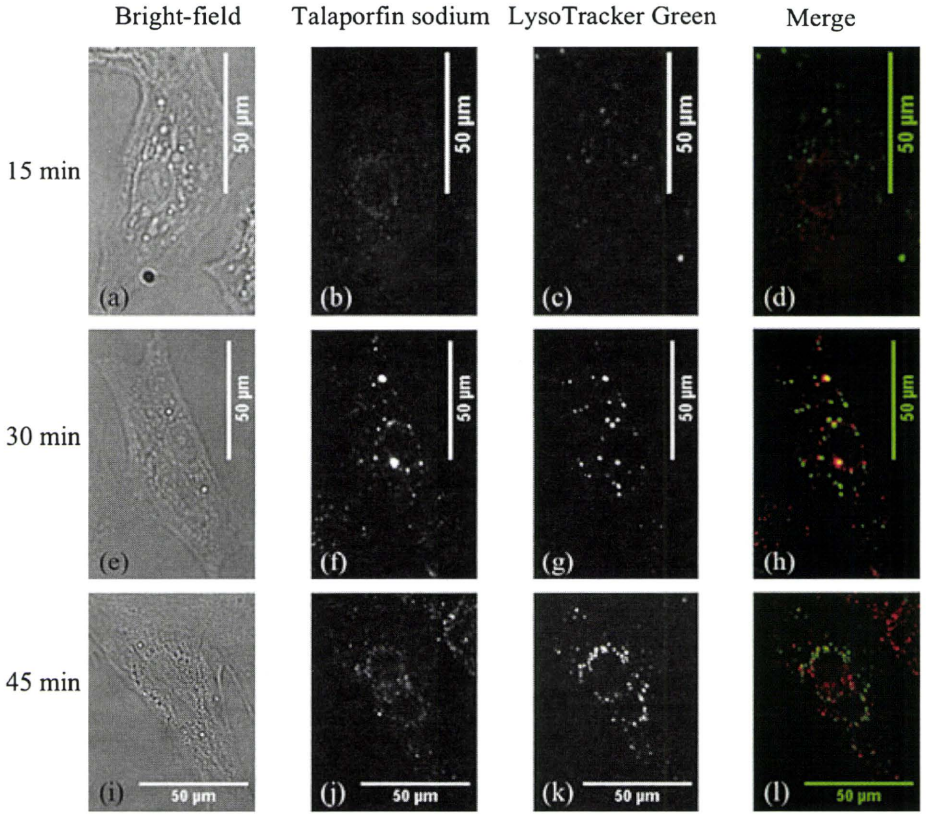

Figure 4. Intracellular talaporfin sodium distribution in rat myocardial cells. The cells were incubated in the medium containing talaporfin sodium (30 μg mL^{-1}) for 15 min [(a)–(d)], 30 min [(e)–(h)] and 45 min [(i)–(l)]. From left to right, bright-field image, talaporfin sodium fluorescence image, LysoTracker Green fluorescence image and the merged image of talaporfin sodium fluorescence and LysoTracker Green fluorescence.

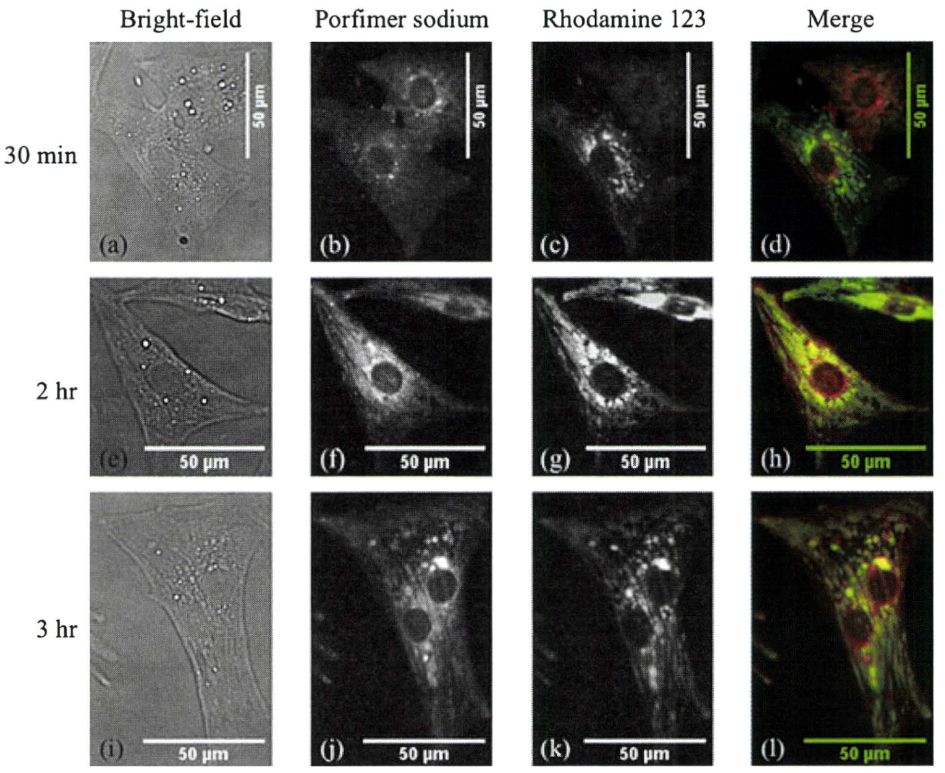

Figure 5. Intracellular porfimer sodium distribution in rat myocardial cells. Cells were incubated in the medium containing porfimer sodium (30 μg mL^{-1}) for 30 min [(a)–(d)], 2 h [(e)–(h)] and 3 h [(i)–(l)]. From left to right, bright-field image, porfimer sodium fluorescence image, Rhodamine 123 fluorescence image and the merged image of porfimer sodium fluorescence and Rhodamine 123 fluorescence.

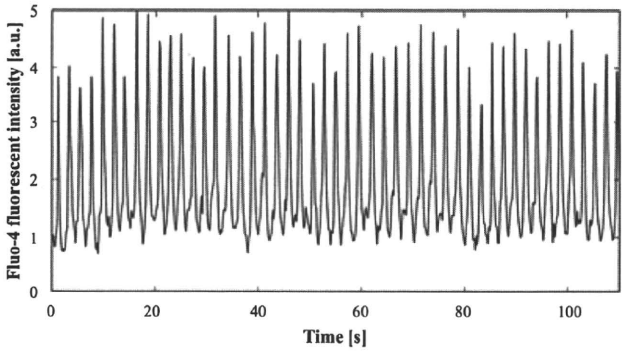

Figure 6. Changes in the control Fluo-4 fluorescence intensity without irradiation and with talaporfin sodium at 15 min loading.

almost uniform dim light of porfimer sodium fluorescence in all cells indicates that porfimer sodium was distributed in the cell membrane. The similarity between the fluorescence images of porfimer sodium and Rhodamine 123 was observed over 2–3 h of incubation (Fig. 5h,l). These results indicate that porfimer sodium distributed on the cell membrane at first for several tens of minutes of incubation and then relocalized to the mitochondria after several hours of further incubation.

Intracellular Ca^{2+} concentrations during the photosensitization reaction with talaporfin sodium or porfimer sodium

The acute subsecond response of intracellular free Ca^{2+} concentration ($[Ca^{2+}]_{in}$) of the myocardial cells to the exogenous photosensitization reaction with talaporfin sodium or porfimer sodium for a short period of photosensitizer incubation (15 min) was measured by using a confocal laser microscope. The time courses of the change in normal Fluo-4 fluorescence intensity in single myocardial cells are shown in Fig. 6, with the control condition being the presence of photosensitizer and the absence of photoactivation. The change in normal Fluo-4 fluorescence intensity of single myocardial cells was obtained as a control during the measurement period of 110 s. The well-known periodic change in intracellular Ca^{2+} concentration accompanied by excitation and contraction processes of myocardial cells, the so-called Ca^{2+} oscillation, was observed as the periodic increase and decrease in Fluo-4 fluorescence intensity (data not shown). The periodic change in Fluo-4 fluorescence intensity was not influenced by the addition of talaporfin sodium to the control (Fig. 6); the same result was obtained with porfimer sodium. There was almost no Fluo-4 photobleaching in this experimental setting during the measurement period. The laser used for Fluo-4 excitation was found to have less influence on the measurement of Fluo-4 fluorescence during the photosensitization reaction.

Figure 7a,b shows the change in Fluo-4 fluorescence intensity in single myocardial cells during the exogenous photosensitization reaction after the short period of incubation with talaporfin sodium (Fig. 7a) and porfimer sodium (Fig. 7b). A similar temporal pattern in the recorded change in Fluo-4 fluorescence intensity between both photosensitizers was observed when the photosensitizer was mainly located outside the cells. Soon after the start of irradiation, the amplitude of the periodic oscillation in the Fluo-4 fluorescence intensity

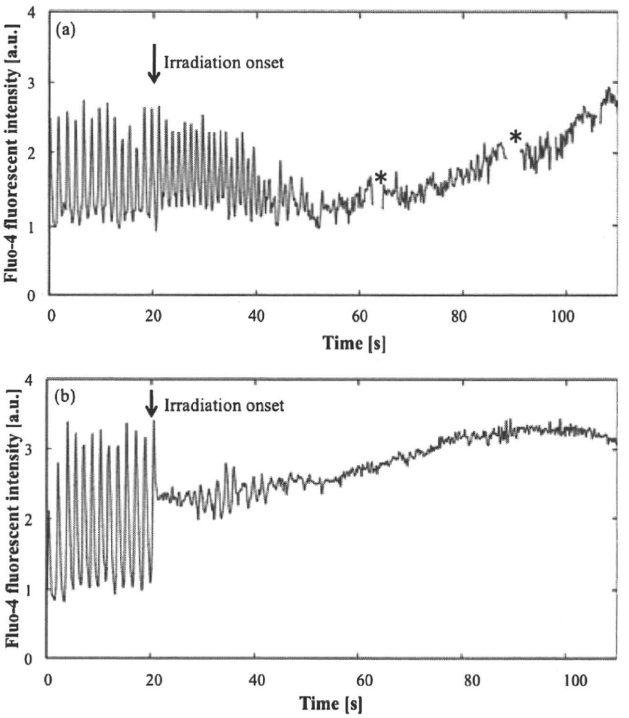

Figure 7. Changes in Fluo-4 fluorescence intensity during the exogenous photosensitization reaction after a short period of incubation with (a) talaporfin sodium and (b) porfimer sodium. The asterisks shown in the graph indicate the break for the focus adjustment.

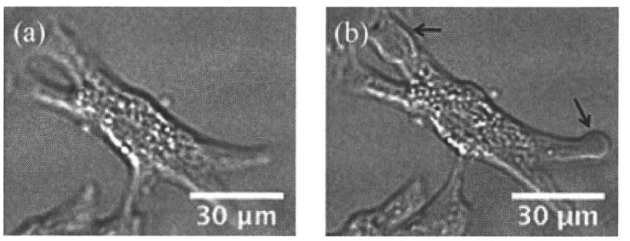

Figure 8. Morphological change (a) before and (b) 5 min after the photosensitization reaction with talaporfin sodium in a certain cell. The arrows shown in (b) indicate bleb formation.

disappeared within a few seconds. A subsequent irradiation induced a gradual increase in $[Ca^{2+}]_{in}$, which eventually exceed the maximum value in the normal oscillation. A drastic morphology change after the photosensitization reaction for the short period of incubation with talaporfin sodium, such as bleb formation, was observed on the surface of the myocardial cells without visible damage to the nuclei (Fig. 8), which was also observed in the reaction with porfimer sodium. However, there were differences in the extent of temporal response of the Fluo-4 fluorescence intensity to the photosensitization reaction between the photosensitizers. The time required for the oscillation amplitude to disappear was longer in the reaction with talaporfin sodium than that with porfimer sodium. A gentle slope in the temporal Fluo-4 fluorescence intensity change was obtained with talaporfin sodium.

In contrast, the photosensitization reaction with the photosensitizers distributed in the intracellular compartment showed a difference in the temporal tendency of the electrophysiological

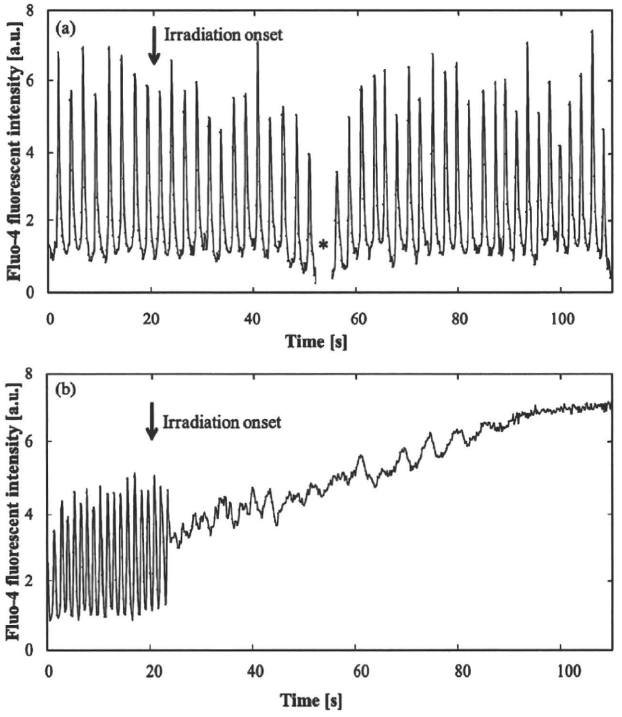

Figure 9. Changes in Fluo-4 fluorescence intensity during photosensitization reaction after a long period of incubation with (a) talaporfin sodium and (b) porfimer sodium. The asterisks shown in the graph indicate the break for the focus adjustment.

response between talaporfin sodium and porfimer sodium (Fig. 9a,b). Little change in the periodic oscillation of fluorescence intensity was observed with the photosensitization reaction in the long period of incubation with talaporfin sodium (Fig. 9a), indicating that the damage in the intracellular compartment, especially in lysosomes, might cause almost no acute effect on the electrophysiological cellular function. On the other hand, the photosensitization reaction in the long period of incubation with porfimer sodium induced the same response as in the short period of the photosensitizer incubation (Fig. 9b).

DISCUSSION

The subsecond intracellular calcium responses of rat myocardial cells to the photosensitization reaction for a short period of photosensitizer incubation showed similar temporal tendencies between both photosensitizers, talaporfin sodium and porfimer sodium (Fig. 7). The temporal characteristics of the Fluo-4 fluorescence intensity triggered by the photosensitization reaction could be divided into two phases: the first phase was the disappearance of Ca^{2+} oscillation, called the "phase I acute response," and the second phase was the gradual increase in $[Ca^{2+}]_{in}$, called the "phase II slow response." The regular spike showing normal activity of myocardial cells obtained before irradiation disappeared within the first several tens of seconds after the onset of photoactivation. This acute response might be caused by ion channel dysfunction because no microscopically significant cell morphological change was observed. After the disappearance of automaticity, there was a brief period of relatively constant level of Fluo-4 fluorescence

Table 1. The experimentally obtained decay time of the Ca^{2+} oscillation amplitude and average rate of change in $[Ca^{2+}]_{in}$ in various conditions.

	Talaporfin sodium		Porfimer sodium	
	Short period incubation	Long period incubation	Short period incubation	Long period incubation
Decay time of the Ca^{2+} oscillation amplitude (s)	11	-*	9.9	6.8
Average rate of change in $[Ca^{2+}]_{in}$ (nM s^{-1})	20.1	-*	44.5	82.9

*In the condition of long period of incubation with talaporfin sodium, there was almost no cellular response in $[Ca^{2+}]_{in}$ to the photosensitization reaction during the measurement period up to 200 s, so that the decay time and the average rate of $[Ca^{2+}]_{in}$ change defined as above definitions is not calculated.

intensity, followed by a gradual increase in Fluo-4 fluorescence intensity as the phase II slow response occurs. The elevation of the Fluo-4 fluorescence intensity in phase II is possibly induced by the Ca^{2+} influx due to the difference in Ca^{2+} concentration between inside and outside the cell. The Ca^{2+} influx and cell morphological changes such as bleb formation indicate that the photosensitization reaction in the short period of incubation might cause cell membrane damage, mostly micropore formation on the surface of the cell membrane.

To compare the early electrophysiological cellular response to the photosensitization reaction between the photosensitizers and between their distributions, the temporal characteristic of the change in intracellular Ca^{2+} concentration with the photosensitization reaction was examined in both the phase I acute response and the phase II slow response. We focused on one parameter in each phase. The first one in the phase I acute response is "decay time of the Ca^{2+} oscillation amplitude," which is defined as the time required for the oscillation amplitude in the Fluo-4 fluorescence intensity to decrease to 1/e of the pre-irradiation average value after the onset of the irradiation. The oscillation amplitude in the fluorescence intensity was defined as the difference between the maximum and minimum fluorescence intensities during the oscillation period obtained before the onset of irradiation. The oscillation amplitude decreased with time during the photosensitization reaction. The decay times of the oscillation amplitude in the three conditions, talaporfin sodium with a short period of incubation and porfimer sodium with a short/long period of incubation, are shown in Table 1. The decay time was longer in the photosensitization reaction with talaporfin sodium than that with porfimer sodium.

The second parameter is "average rate of change in $[Ca^{2+}]_{in}$" in the phase II slow response. After the oscillation disappearance followed by a brief period of relatively constant level in $[Ca^{2+}]_{in}$, then $[Ca^{2+}]_{in}$ began to increase with time. We define "average rate of change in $[Ca^{2+}]_{in}$" during about 20 s after the initiation of the $[Ca^{2+}]_{in}$ increase. To obtain the average rate of change in $[Ca^{2+}]_{in}$, the estimated intracellular Ca^{2+} concentration was calculated from the measured Fluo-4 fluorescence intensity in the range of the normal oscillation amplitude using the following equation (33).

$$[Ca^{2+}]_{in} = K_d \frac{F - F_{min}}{F_{max} - F} \quad (1)$$

where K_d is the dissociation constant of Fluo-4 reported to be 345 nM (32,34), F_{min} is the Fluo-4 fluorescence intensity in the absence of Ca^{2+}, F_{max} is the fluorescence intensity in saturated Ca^{2+} and F is the fluorescence intensity in intermediate Ca^{2+} levels. We assume that F_{min} is zero to calculate the intracellular Ca^{2+} concentration from Eq (1). The fluorescence intensity is normalized by the minimum value of the oscillation intensity before the irradiation onset, where $[Ca^{2+}]_{in}$ is assumed to be 100 nM (35). The average rate of change in $[Ca^{2+}]_{in}$ was obtained from the changes in $[Ca^{2+}]_{in}$ during the photosensitization reaction calculated using Eq (1). We assume that these gradual increases in $[Ca^{2+}]_{in}$ several tens of seconds after the initiation of $[Ca^{2+}]_{in}$ increase might be caused by the micropores formed on the cell membrane in the early stage of the photosensitization reaction and then by the Ca^{2+} influx through the micropores (13). The amount of the photosensitizer and oxygen might be restricted by the limited volume of our experimental setup; thus, oxygen might be possibly exhausted during the early stage of the photosensitization reaction. The initial oxygen concentration in the medium might correspond to 220 μM in the air-saturated solution at 25°C. The oxygen concentration of the photosensitizer solution might have suddenly decreased at the onset of the photosensitization reaction. Several observation of the exhaustion of oxygen during photosensitization reaction has been reported. For example, our research group has reported that oxygen concentration was decreased to 40% of the initial value after the photosensitization reaction with 6.0 μg mL^{-1} talaporfin sodium solution in the condition when the fluence was 1 J cm^{-2} and fluence rate was 200 mW cm^{-2} with a red diode laser (CW, λ = 670 nm) (29). We assume that a certain number of micropores might be formed in the photosensitization reaction with a limited amount of O_2 and then Ca^{2+} influx through the micropores might occur due to the difference in intracellular and extracellular Ca^{2+} concentrations. Table 1 shows the experimentally obtained average rate of change in $[Ca^{2+}]_{in}$ in three conditions: in the short period of incubation with talaporfin sodium and in the short/long period of incubation with porfimer sodium. The photosensitization reaction in the short period of incubation with porfimer sodium is found to induce twice as high average rate of change in $[Ca^{2+}]_{in}$ as with talaporfin sodium.

The shorter decay time of the Ca^{2+} oscillation amplitude (Table 1) and the higher average rate of change in $[Ca^{2+}]_{in}$ (Table 1) were obtained in the photosensitization reaction with porfimer sodium. We think that the parameter in phase I acute response, decay time of the Ca^{2+} oscillation amplitude, indicate the extent of the damage in cellular electrophysiological function such as ion channel malfunction and the other parameter in phase II slow response, average rate of change in $[Ca^{2+}]_{in}$, indicate the extent of the damage in cell membrane such as micropore formation. The results (Table 1) indicate that the earlier cellular response to the photosensitization reaction and the higher efficiency in membrane damage might be obtained with porfimer sodium than with talaporfin sodium. In our experimental condition, the molar energy of absorption per unit volume per unit time was higher with talaporfin sodium (2.8×10^3 J s^{-1} M^{-1} cm^{-3}) than with porfimer sodium (3.4×10^2 J s^{-1} M^{-1} cm^{-3}). Talaporfin sodium has been reported to have a larger triplet quantum yield than porfimer sodium (36), while the triplet state quenching rate is almost the same between the two photosensitizers: 1.3×10^9 M^{-1} s^{-1} for talaporfin sodium (37) and $1.4–1.8 \times 10^9$ M^{-1} s^{-1} for porfimer sodium (38–40). The singlet oxygen quantum yield in talaporfin sodium, 0.77 (37), is larger than that in HPD, 0.06–0.63 (38,41). Despite the higher singlet oxygen quantum yield and the higher molar energy of absorption in the photosensitization reaction with talaporfin sodium, our experimental results indicate that the slower response rate and lower efficiency in micropore formation might be affected by another factor, which might be the photosensitizer location. The photocytotoxic process depends on the distance between the photosensitizer and target cell or subcellular compartment due to the short diffusion path of the singlet oxygen during the lifetime (< 4 μs) in aqueous medium (42). In our experimental condition of short or long period of incubation with porfimer sodium, the lipophilic porfimer sodium might be located on and/or inside the cell membrane (Fig. 5). Lipophilic porphyrins have been reported to generate $^1O_2$ within the membrane bilayer in photoactivation, which might cause membrane protein damage, resulting in electric depolarization, increased permeability, membrane rupture and cell lysis (43–45). The intrinsic lifetime of $^1O_2$ has been reported to be relatively long (13–35 μs) in the lipid bilayer (46,47). Moreover, the membrane-bound porfimer sodium might cause lipid peroxidation effectively in type I reactions (48). In our experimental condition of long period of incubation, a large number of porfimer sodium molecules might be located between the lipid bilayer; thus, the porfimer sodium binding to cell membrane bilayer could induce a more effective micropore formation than that in the short period of incubation. On the other hand, the hydrophilic talaporfin sodium could not bind to the cell membrane; thus, its distance from the cell membrane might be longer than that of porfimer sodium. The singlet oxygen generated from the photoactivation of talaporfin sodium might interact with the cell membrane within an activation length. The activation length might be a diffusion radius of singlet oxygen during the lifetime, reported to be < 220 nm in aqueous solution (49). In our experimental condition for a short period of incubation with talaporfin sodium, the generated singlet oxygen, which might exist within the activation distance from the cell membrane, could cause micropore formation. Despite the long distance from the cell membrane, the higher amounts of singlet oxygen generated in the photosensitization reaction with talaporfin sodium might cause the same level of photocytotoxicity as with porfimer sodium. No electrical responses were observed in the condition of long period of incubation (Fig. 9a). Since talaporfin sodium was localized to the subcellular compartment, especially in the lysosome (Fig. 4), the singlet oxygen might be generated inside the lysosome. The activation path length of the singlet oxygen in the cell has been reported to be 10–20 nm (50,51). The singlet oxygen generated inside the lysosome might cause focal damage of the lysosome, resulting to apoptotic cell death.

In this study, we found that exogenous photosensitization reactions for a short period of photosensitizer incubation induce acute electrophysiological cellular responses and cell membrane damage with similar temporal tendencies between two photosensitizers; talaporfin sodium and porfimer sodium.

We also found that the photocytotoxic process differs between the two photosensitizers, with the main difference being the distance between the photosensitizers and their target (i.e. the cell membrane). The lipophilic porfimer sodium might cause direct membrane damage with small amounts of generated singlet oxygen, while the hydrophilic talaporfin sodium might cause the same level of damage to the cell membrane with large amounts of generated singlet oxygen.

Acknowledgements—This study was partially supported by the Supporting Program for Creating University Ventures (#1904) of the Japan Science and Technology Agency and by Research Fellowships of the Japan Society for the Promotion of Science for Young Scientists.

REFERENCES

1. Dougherty, T. J., C. J. Gomer, B. W. Henderson, G. Jori, D. Kessel, M. Korbelik, J. Moan and Q. Peng (1998) Photodynamic therapy (Review). *J. Natl Cancer Inst.* **90**, 889–905.
2. Schuitmaker, J. J., P. Baas, H. L. L. M. van Leengoed, F. W. van der Meulen, W. M. Star and N. van Zandwijk (1996) Photodynamic therapy: A promising new modality for the treatment of cancer. *J. Photochem. Photobiol. B, Biol.* **34**, 3–12.
3. Dougherty, T. J. (1993) Photodynamic therapy. *Photochem. Photobiol.* **58**, 895–900.
4. Oleinick, N. L., R. L. Morris and I. Belichenko (2002) The role of apoptosis in response to photodynamic therapy: What, where, why, and how. *Photochem. Photobiol. Sci.* **1**, 1–21.
5. Moore, J. V., C. M. L. West and C. Whitehurst (1997) The biology of photodynamic therapy. *Phys. Med. Biol.* **42**, 913–935.
6. Buytaert, E., M. Dewaele and P. Agostinis (2007) Molecular effectors of multiple cell death pathways initiated by photodynamic therapy. *Biochim. Biophys. Acta* **1776**, 86–107.
7. Spikes, J. D. and J. C. Bommer (1993) Photobleaching of mono-L-aspartyl chlorin e6 (NPe6): A candidate sensitizer for the photodynamic therapy of tumors. *Photochem. Photobiol.* **58**, 346–350.
8. Delinger, M. (1996) Apoptosis or necrosis following Photofrin® photosensitization: Influence of the incubation protocol. *Photochem. Photobiol.* **64**, 182–187.
9. Kessel, D., Y. Luo, Y. Deng and C. K. Chang (1997) The role of subcellular localization in initiation of apoptosis by photodynamic therapy. *Photochem. Photobiol.* **65**, 422–426.
10. Kessel, D., M. Castelli and J. Reiners Jr. (2002) What are the targets of photodynamic therapy? *Proc. SPIE* **4612**, 122–127.
11. Stark, G. (2005) Functional consequences of oxidative membrane damage. *J. Membr. Biol.* **205**, 1–16.
12. Zhou, Z., H. Yang and Z. Zhang (2003) Role of calcium in phototoxicity of 2-butylamino-2-demethoxy-hypocrellin A to human gastric cancer MGC-803 cells. *Biochim. Biophys. Acta* **1593**, 191–200.
13. Specht, K.G. and M. A. J. Rodgers (1991) Plasma membrane depolarization and calcium influx during cell injury by photodynamic action. *Biochim. Biophys. Acta* **1070**, 60–68.
14. Hubmer, A., A. Hermann, K. Uberreigler and B. Krammer (1996) Role of calcium in photodynamically induced cell damage of human fibroblasts. *Photochem. Photobiol.* **64**, 211–215.
15. Zong, W. X. and C. B. Thompson (2006) Necrotic death as a cell fate. *Genes Dev.* **20**, 1–15.
16. Bers, D. M. (2002) Cardiac excitation–contraction coupling. *Nature* **415**, 198–205.
17. Douplik, A., A. A. Stratonnikov, V. B. Loschchenov, V. S. Lebedeva, V. M. Derkacheva, A. Vitkin, V. D. Rumyanceva, S. G. Kusmin, A. F. Mironov and E. A. Luk'Yanets (2000) Study of photodynamic reactions in human blood. *J. Biomed. Opt.* **5**, 338–349.
18. Tarr, M., A. Frolov and D. P. Valenzeno (2001) Photosensitization-induced calcium overload in cardiac cells: Direct link to membrane permeabilization and calcium influx. *Photochem. Photobiol.* **72**, 418–424.
19. Ito, A., S. Hosokawa, S. Miyoshi, K. Soejima, S. Ogawa and T. Arai (2010) The myocardial electrical blockade induced by photosensitization reaction. *IEEE Trans. Biomed. Eng.* **57**, 488–495.
20. Penning, L. C., M. H. Rasch, E. Ben-Hur, T. M. A. R. Dubbelman, A. C. Havelaar, J. Van der Zee and J. Van Steveninck (1992) A role for transient increase of cytoplasmic free calcium in cell rescue after photodynamic treatment, *Biochim. Biophys. Acta* **1107**, 255–260.
21. Pass, H. I. (1993) Photodynamic therapy in oncology: Mechanisms and clinical use. *J. Natl Cancer Inst.* **85**, 443–456.
22. Hsieh, Y.J., C. C. Wu, C. J. Chang and J. S. Yu (2003) Subcellular localization of Photofrin® determines the death phenotype of human epidermoid carcinoma A431 cells triggered by photodynamic therapy: When plasma membranes are the main targets. *J. Cell. Physiol.* **194**, 363–375.
23. Aizawa, K., T. Okunaka, T. Ohtani, H. Kawabe, Y. Yasunaka, S. O'Hata, N. Ohtomo, K. Nishimiya, C. Konaka, H. Kato, Y. Hayata and T. Saito (1987) Localization of mono-L-aspartyl chlorin e6 (NPe6) in mouse tissues. *Photochem. Photobiol.* **46**, 789–793.
24. Kato, H., K. Furukawa, M. Sato, T. Okunaka, Y. Kusunoki, M. Kawahara, M. Fukuoka, T. Miyazawa, T. Yana, K. Matsui, T. Shiraishi and H. Horinouchi (2003) Phase II clinical study of photodynamic therapy using mono-image-aspartyl chlorin e6 and diode laser for early superficial squamous cell carcinoma of the lung. *Lung Cancer* **42**, 103–111.
25. Chan, A. L., M. Juarez, R. Allen, W. Volz and T. Albertson (2005) Pharmacokinetics and clinical effects of mono-l-aspartyl chlorin e6 (NPe6) photodynamic therapy in adult patients with primary or secondary cancer of the skin and mucosal surfaces. *Photodermatol. Photoimmunol. Photomed.* **21**, 72–78.
26. Roberts, W. G. and M. W. Berns (1989) In vitro photosensitization I. Cellular uptake and subcellular localization of mono-L-aspartyl chlorin e6, chloro-aluminum sulfonated phthalocyanine, and photofrin II. *Lasers Surg. Med.* **9**, 90–101.
27. Roberts, W. G., L. H. L. Liaw and M. W. Berns (1989) In vitro photosensitization II. An electron microscopy study of cellular destruction with mono-l-aspartyl chlorin e6 and photofrin II. *Lasers Surg. Med.* **9**, 102–108.
28. Reiners Jr, J. J., J. A. Caruso, P. Mathieu, B. Chelladurai, X. M. Yin and D. Kessel (2002) Release of cytochrome c and activation of pro-caspase-9 following lysosomal photodamage involves bid cleavage. *Cell Death Differ.* **9**, 934–944.
29. Ohmori, S., S. Hakomori, T. Tsukahara and T. Arai (2007) A comparative study between pulsed and continuous wave irradiation for Talaporfin sodium mediated photosensitization in solution, in-vitro and in-vivo. *Rev. Laser Eng.* **35**, 180–186.
30. Caruso, J. A., P. A. Mathieu and J. J. Reiners Jr. (2005) Sphingomyelins suppress the targeted disruption of lysosomes/endosomes by the photosensitizer NPe6 during photodynamic therapy. *Biochem. J.* **392**, 325–334.
31. Seguchi, H., M. Ritter, M. Shizukushi, H. Ishida, G. Chokoh, H. Nakazawa, K. W. Spitzer and W. H. Barry (2005) Propagation of Ca^{2+} release in cardiac myocytes: Role of mitochondria. *Cell Calcium* **38**, 1–9.
32. Gee, K. R., K. A. Brown, W. N. U. Chen, J. Bishop-Stewart, D. Gray and I. Johnson (2000) Chemical and physiological characterization of fluo-4 Ca^{2+} indicator dyes. *Cell Calcium* **27**, 97–106.
33. Minta, A., J. P. Kao and R. Y. Tsien (1989) Fluorescent indicators for cytosolic calcium based on rhodamine and fluorescein chromophores. *J. Biol. Chem.* **264**, 8171–8178.
34. Haugland, R. P. (1996) *Handbook of Fluorescent Probes and Research Chemicals*. 6th edn, 505 pp. Molecular Probes Inc., Eugene, OR.
35. Berridge, M. J., P. Lipp and M. D. Bootman (2000) The versatility and universality of calcium signaling. *Nat. Rev. Mol. Cell Biol.* **1**, 11–21.
36. Ohmori, S. and T. Arai (2006) In vitro behavior of Porfimer sodium and Talaporfin sodium with high intensity pulsed irradiation. *Lasers Med. Sci.* **21**, 213–223.
37. Spikes, J. D. and J. C. Bommer (1993) Photosensitizing properties of mono-L-aspartyl chlorin e6 (NPe6): a candidate sensitizer for

the photodynamic therapy of tumors. *J. Photochem. Photobiol. B, Biol.* **17**, 135–143.
38. Reddi, E., M. A. Rodgers and G. Jori (1984) Photophysical and photosensitizing properties of hematoporphyrin bound with human serum albumin. *Prog. Clin. Boil. Res.* **170**, 373–379.
39. Sterenborg, H. and M. J. C. Gemert (1996) Photodynamic therapy with pulsed light sources: A theoretical analysis. *Phys. Med. Biol.* **41**, 835–849.
40. Bonnett, R., C. Lambert, E. J. Land, P. A. Scourides, R. S. Sinclair and T. G. Truscott (1983) The triplet and radical species of haematoporphyrin and some of its derivatives. *Photochem. Photobiol.* **38**, 1–8.
41. Blum, A. and L. I. Grossweiner (1985) Singlet oxygen generation by hematoporphyrin IX, uroporphyrin I and hematoporphyrin derivative at 546 nm in phosphate buffer and in the presence of egg phosphatidylcholine liposomes. *Photochem. Photobiol.* **41**, 27–32.
42. Merkel, P. B. and D. R. Kearns (1972) Radiationless decay of singlet molecular oxygen in solution. Experimental and theoretical study of electronic-to-vibrational energy transfer. *J. Am. Chem. Soc.* **94**, 7244–7253.
43. Ehrenberg, B., E. Gross, Y. Nitzan and Z. Malik (1993) Electric depolarization of photosensitized cells: Lipid vs. protein alterations. *Biochim. Biophys. Acta* **1151**, 257–264.
44. Kessel, D. (1984) Hematoporphyrin and HPD: photophysics, photochemistry and phototherapy. *Photochem. Photobiol.* **39**, 851–859.
45. Dubbelman, T., A. De Goeij and J. Van Steveninck (1978) Protoporphyrin-sensitized photodynamic modification of proteins in isolated human red blood cell membranes. *Photochem. Photobiol.* **28**, 197–204.
46. Ehrenberg, B., J. L. Anderson and C. S. Foote (1998) Kinetics and yield of singlet oxygen photosensitized by hypericin in organic and biological media. *Photochem. Photobiol.* **68**, 135–140.
47. Henderson, B. W. and T. J. Dougherty (1992) How dose photodynamic therapy work? *Photochem. Photobiol.* **55**, 145–157.
48. Athar, M., H. Mukhtar and D. R. Bickers (1998) Differential role of reactive oxygen intermediates in photofrin-I- and photofrin-II-mediated photoenhancement of lipid peroxidation in epidermal microsomal membranes. *J. Invest. Dermatol.* **90**, 652–657.
49. Redmond, R. W. and I. E. Kochevar (2006) Spatially resolved cellular responses to singlet oxygen. *Photochem. Photobiol.* **82**, 1178–1186.
50. Moan, J. and K. Berg (1991) The photodegradation of porphyrins in cells can be used to estimate the lifetime of singlet oxygen. *Photochem. Photobiol.* **53**, 549–553.
51. Moan, J. (1990) On the diffusion length of singlet oxygen in cells and tissues. *J. Photochem. Photobiol. B, Biol.* **6**, 343–347.

STEM CELLS

TRANSLATIONAL AND CLINICAL RESEARCH

Pretreatment of Human Mesenchymal Stem Cells with Pioglitazone Improved Efficiency of Cardiomyogenic Transdifferentiation and Cardiac Function

DAISUKE SHINMURA,[a] IKUKO TOGASHI,[a] SHUNICHIRO MIYOSHI,[a] NOBUHIRO NISHIYAMA,[a] NAOKO HIDA,[a] HIROKO TSUJI,[a] HIKARU TSURUTA,[a] KAORU SEGAWA,[b] YUIKO TSUKADA,[c] SATOSHI OGAWA,[a] AKIHIRO UMEZAWA[d]

[a]Department of Cardiology, [b]Department of Microbiology and Immunology, and [c]Department of Hematology, Keio University School of Medicine, Tokyo, Japan, [d]Department of Reproductive Biology and Pathology, National Research Institute for Child Health and Development, Tokyo, Japan

Key Words. Cardiac • Cell culture • Cell transplantation • Immune-deficient models • Somatic stem cells • Stem cell plasticity • Transdifferentiation

ABSTRACT

The efficacy of transplantation of default human marrow-derived mesenchymal stem cells (MSCs) was modest. In this study, our challenge was to improve the efficacy of MSC transplantation in vivo by pretreatment of MSCs with pioglitazone. MSCs were cultured with or without medium containing 1 μM of pioglitazone before cardiomyogenic induction. After cardiomyogenic induction in vitro, cardiomyogenic transdifferentiation efficiency (CTE) was calculated by immunocytochemistry using anti-cardiac troponin-I antibody. For the in vivo experiments, myocardial infarction (MI) at the anterior left ventricle was made in nude rats. Two weeks after MI, MSCs pretreated with pioglitazone (p-BM; $n = 30$) or without pioglitazone (BM; $n = 17$) were injected, and then survived for 2 weeks. We compared left ventricular function by echocardiogram and immunohistochemistry to observe cardiomyogenic transdifferentiation in vivo. Pretreatment with pioglitazone significantly increased the CTE in vitro (1.9% ± 0.2% $n = 47$ vs. 39.5% ± 4.7% $n = 13$, $p < .05$). Transplantation of pioglitazone pretreated MSCs significantly improved change in left ventricular % fractional shortening (BM; −4.8% ± 2.1%, vs. p-BM; 5.2% ± 1.5%). Immunohistochemistry revealed significant improvement of cardiomyogenic transdifferentiation in p-BM in vivo (BM; 0% ± 0% $n = 5$, vs. p-BM; 0.077% ± 0.041% $n = 5$). Transplantation of pioglitazone-pretreated MSCs significantly improved cardiac function and can be a promising cardiac stem cell source to expect cardiomyogenesis. *STEM CELLS 2011; 29:357–366*

Disclosure of potential conflicts of interest is found at the end of this article.

INTRODUCTION

Cardiac stem cell therapy is a promising therapy for patients with severe heart failure; however, it is still less-developed. One of the critical problems is absence of ready-to-use stem cell sources. Embryonic stem cells [1] or induced pluripotent stem cells [2] have cardiomyogenic differentiation potential and are major candidates for future stem cell therapy, but, there are still several problems to overcome before clinical application, that is, neoplasm formation [3] and chromosomal stability [4]. Human bone marrow-derived mesenchymal stem cells (BM-MSCs) have a cardiomyogenic transdifferentiation ability; however, the cardiomyogenic transdifferentiation efficiency (CTE) is extremely low [5]. Residential cardiac precursor cells [6], having a mesenchymal phyenotype [7], have a higher CTE potential in comparison with BM-MSCs, but may not be so high in comparison with the other types of human mesenchymal cells, that is, umbilical cord blood-derived (UCB-MSC) [8], menstrual blood-derived (MMC) [9], placental chorionic plate-derived MSC (PCPCs) [10], and amniotic membrane-derived MSC (AMCs) [11]. Moreover, these mesenchymal cells are expected to be used in an allograft manner and not as ready-to-use materials until the establishment of a stem cell bank system that will cover all major histocompatibility complexes to avoid rejection. Among these human

Author contributions: D.S.: conception and design, collection and assembly of data, final approval of manuscript; I.T.: conception and design, collection and assembly of data, final approval of manuscript; S.M.: conception and design, administrative support, collection and assembly of data, data analysis and interpretation, manuscript writing, final approval of manuscript; N.N.: conception and design, collection and assembly of data, final approval of manuscript; N.H.: conception and design, collection and assembly of data; H. Tsuji: conception and design, collection and assembly of data, final approval of manuscript; H. Tsuruta: conception and design, collection and assembly of data, final approval of manuscript; K.S.: conception and design, collection and assembly of data, final approval of manuscript; Y.T.: provision of study material or patients, collection and assembly of data, final approval of manuscript; S.O.: financial support, administrative support, final approval of manuscript; A.U.: financial support, administrative support, final approval of manuscript. D.S. and I.T. contributed equally to this article.

Correspondence: Shunichiro Miyoshi, M.D., Ph.D., Keio University School of Medicine, 35-Shinanomachi, Shinjuku-ku, Tokyo 1608582, Japan. Telephone: 81-3-3353-1211 (ext 62310); Fax: 81-3-3353-2502; e-mail: smiyoshi@cpnet.med.keio.ac.jp Received June 3, 2010; accepted for publication November 17, 2010; first published online in STEM CELLS *EXPRESS* December 9, 2010. 1066-5099/2009/$30.00/0 doi: 10.1002/stem.574